EFDA–JET–PR(10)22

E. Delabie, M. Brix, R.J.E. Jaspers, C. Giroud, O. Marchuk, M.G. O'Mullane,
Yu Ralchenko, E. Surrey, M.G von Hellermann, K.D. Zastrow
and JET EFDA contributors

Consistency of Atomic Data for the Interpretation of Beam Emission Spectra

Consistency of Atomic Data for the Interpretation of Beam Emission Spectra

E. Delabie[1], M. Brix[2], R.J.E. Jaspers[3], C. Giroud[2], O. Marchuk[4], M.G. O'Mullane[5], Yu Ralchenko[6], E. Surrey[2], M.G von Hellermann[1], K.D. Zastrow[2] and JET EFDA contributors*

JET-EFDA, Culham Science Centre, OX14 3DB, Abingdon, UK

[1]FOM Institute for Plasma Physics Rijnhuizen, Association EURATOM-FOM, P.O. Box 1207, 3430 BE Nieuwegein, The Netherlands
[2]EURATOM-CCFE Fusion Association, Culham Science Centre, OX14 3DB, Abingdon, OXON, UK
[3]Eindhoven University of Technology, Postbus 513, 5600 MB Eindhoven, The Netherlands
[4]Forschungszentrum Jülich, Association EURATOM-FZJ, 52425, Jülich, Germany
[5]Department of Physics, University of Strathclyde, 107 Rottenrow, Glasgow G4 0NG, UK
[6]Atomic Physics Division, National Institute of Standards and Technology, Gaithersburg, MD 20899-8422, USA
** See annex of F. Romanelli et al, "Overview of JET Results", (Proc. 22[nd] IAEA Fusion Energy Conference, Geneva, Switzerland (2008)).*

Preprint of Paper to be submitted for publication in
Plasma Physics and Controlled Fusion

ABSTRACT.
Several Collisional-Radiative (CR) models [1, 2, 3] have been developed to calculate the attenuation and the population of excited states of hydrogen or deuterium beams injected into tokamak plasmas. The datasets generated by these CR models are needed for the modelling of beam ion deposition and (excited) beam densities in current experiments, and the reliability of this data will be crucial to obtain helium ash densities on ITER combining charge exchange and beam emission spectroscopy. Good agreement between the different CR models for the Neutral Beam (NB) is found, if corrections to the fundamental cross sections are taken into account. First the H_α and H_β beam emission spectra from JET are compared with the expected intensities. Second, the line ratios within the Stark multiplet are compared with the predictions of a sublevel resolved model. The measured intensity of the full multiplet is ≈30% lower than expected on the basis of beam attenuation codes and the updated beam emission rates, but apart from the atomic data this could also be due to the characterization of the NB path and line of sight integration and the absolute calibration of the optics. The modelled $n = 3$ to $n = 4$ population agrees very well with the ratio of the measured H_α to H_β beam emission intensities. Good agreement is found as well between the neutral beam power fractions measured with beam emission in plasma and on the JET Neutral Beam Test Bed. The Stark line ratios and σ/π intensity ratio deviate from a statistical distribution, in agreement with the CR model in parabolic states from Marchuk et al. [4].

1. MOTIVATION

Powerful neutral hydrogen or deuterium beams provide the dominant external heating and momentum input in most large scale tokamak experiments. For the interpretation of neutral beam (NB) heated discharges, detailed knowledge is required about the energy distribution of the neutrals (power fractions) and the attenuation of the beams in order to obtain radial proles of the fast ion deposition and hence of the heating, torque and beam driven current. For the quantitative interpretation of Charge eXchange (CX) spectra, the local NB fluxes and population of excited states in the beam are needed to convert CX emissivities into local impurity densities. All these calculations strongly rely on the accuracy of the atomic data for the NB that is provided by Collisional-Radiative (CR) models of the beam [1, 2, 3, 5, 6].

When the Beam Emission Spectrum (BES) was recorded for the first time, it was immediately proposed to monitor the beam attenuation, and hence the accuracy of the effective beam stopping cross sections, by using the observed beam emission intensities [7, 8]. This replaces the accumulated error on the beam attenuation along the beam path [9], by a local error in the beam emission rate. Beam emission, when combined with Charge eXchange Recombination Spectroscopy (CXRS), also has the potential of reducing the need of an absolute calibration of the CXRS spectra and a calculation of the intersection integral between a line of sight and the NB, to a relative calibration between several spectral bands [8, 10, 11]. The combination of BES and CXRS is the only feasible method to measure helium ash concentrations with the requested accuracy on ITER where only a small fraction (≈1%) of the diagnostic beam reaches the plasma center and where calibrations of

the tokamak side optics on a regular basis will be impossible [12]. The beam emission intensity and Doppler shift is also widely used to characterise the beam (power fractions [9, 13, 14], alignment [15], divergence [14]).

Apart from using the intensity of the full BES multiplet, the σ/π intensity ratio [9, 16, 17, 12] and Stark splitting [18, 19] can be used as an alternative to polarisation based Motional Stark effect (MSE) diagnostics, as proposed for the ITER diagnostic and heating beam respectively. For these applications the Stark level population structure of the beam neutrals is required to model the spectra, like for polarisation based MSE diagnostics when σ and π-lines overlap.

Despite these promising applications, the use of beam emission has been hampered by the reliability of the involved atomic data and the complexity of the spectra. At the same time, the modelled NB fast ion deposition has been exploited at ever higher accuracy, thereby strongly relying on the accuracy of the underlying beam stopping calculations. It is the aim of this paper to check the consistency of the various beam modelling efforts and to quantitatively compare modelled neutral beam densities with measured beam densities from beam emission on JET.

In section 2 several published CR models for the neutral beam are compared. A distinction is made between models that implicitly assume a statistical population of the Stark levels within an n-shell (section 2.1-2.3) and models that have Stark level resolution (section 2.4). The latter models are mainly useful for the analysis of MSE data. In section 3 measured beam emission intensities from JET are compared to the expected beam densities from the beam stopping calculations. The expected line ratios within the MSE multiplet are compared with experimental data in section 4.

2. ATOMIC MODELS OF THE NEUTRAL BEAM

2.1. COLLISIONAL-RADIATIVE MODELS FOR THE NEUTRAL BEAM (N-RESOLVED)

The first neutral beam models that take excited states into account are by Boley et al. [20] and Janev et al. [5]. The focus of these works was solely on the penetration length of neutral beams. Although beam stopping is mainly determined by direct proton impact ionization and charge exchange from the ground state, excited states become increasingly important with increasing beam energy and plasma density. Seraydarian et al. [7] found relatively good agreement between the measured and predicted beam emission intensity on DIII-D, using a model based on the data of Boley et al. [20]. However, the ion impact excitation cross sections used in [20] were too large, which makes the interpretation of the beam emission results in [7] difficult. Mandl et al. [9] compared the measured and expected beam densities on JET using the ADAS CR model (here referred to as ADAS89). They found relatively good agreement between model and experiment. Anderson et al. [1] thoroughly revisited the ADAS beam model (here referred to as ADAS97) and brought it to a large extent in line with the 1993 review of atomic data by Janev and Smith [21]. The observed intensity on JET was found to be 30% lower than predicted. Hutchinson [2] built a CR model of the beam based on the Janev 1989 and 1993 atomic datasets [5, 21] and found a large discrepancy with ADAS97. Marchuk et al. [3] assessed the atomic data needs for active beam spectroscopy on ITER (based on the Janev 1993 dataset) and found a good agreement between their CR model and ADAS97, but

only compared for the ITER diagnostic beam relevant conditions of 100keV/amu.

2.2. CONSISTENCY OF ATOMIC DATA FOR NB EMISSION

An investigation of the discrepancies between the CR models [1, 2, 3] revealed two issues: (1) The high energy part of the proton impact ionization cross section for excited states published in the Janev 1993 review is based on erroneous input data from [22]. Although this error was noted [23, 24] and corrected by the authors [25], the IAEA recommended data in the Alladin database [26] has not changed yet. A new fit to the ionization cross sections has been made and implemented in the CR models of ADAS (see [27] for details) and Marchuk et al. The different datasets are compared in Fig.1. (2) Furthermore, a bug in the ADAS CR code affected the CX cross sections for excited donor states in hydrogen, strongly affecting the beam emission rates below 100keV/amu. The corrected dataset will here be referred to as ADAS10[1]. The result of these corrections is visually depicted in Fig.2. Both the corrected emission rates of ADAS, Marchuk et al. and Hutchinson agree within 5% for the plasma and beam conditions studied here. The measured beam densities derived from these beam emission rates will be compared with experimental data from JET in section 3.

2.3. CONSISTENCY OF ATOMIC DATA FOR NB STOPPING

The changes mentioned above in the electron loss cross sections from excited states in the neutral beam, and the corresponding uncertainties, have only a small influence on the NB stopping cross sections for current experiments. This is because excited states only contribute ≈20% to the effective beam stopping cross section for JET-like beams and plasmas (50keV/amu, $n_e = 5\times10^{19}$ m^{-3}). For ITER-like beams (500keV/amu, $n_e = 5\times10^{19}$ m^{-3}) however this augments to ≈45%. The models used here do not take ionization by the Lorentz field into account, which is negligible for present experimental conditions but could increase the ionization through excited states even further for the ITER heating beams. In figure 3(a) the increase of the beam stopping cross section due to step wise ionization is shown as a function of electron density for several NB energies. In figure 3(b) beam stopping cross sections from several datasets are compared. The difference between the beam stopping cross sections from ADAS and Marchuk et al. [3] is in all conditions below a few percent. The analytical expressions for the beam stopping cross sections provided by Suzuki et al. [6] are on average 10% higher for current experimental conditions. The 1989 effective beam stopping data from Janev et al. [5], which is based on outdated data compared to the 1993 review by Janev and Smith [21] and is not shown here, is higher by more than 20% but merges with the current data at beam energies of several 100keV/amu. The change between the ADAS10 and ADAS97 beam stopping cross sections is also plotted. The dfference stays below 5%. In conclusion, the different sets of beam stopping data for deuterium plasmas [1, 3, 6] only show a small deviation and are for current experimental conditions dominated by ion impact ionization and charge exchange from the ground state. Changes in the excited population (e.g. Fig. ADAS97 vs. ADAS10) only have a modest impact on beam stopping. It is the accuracy of the fundamental datasets concerning the ground state that determines the overal accuracy of the beam stopping cross sections. The quality

[1] *This data is part of ADAS release v3.1.*

of proton impact ionization from the ground state is classified in category B by the IAEA [26] and charge exchange with low-Z ions is categorised as B-C (B: uncertainty 10-25%, C: 25-50%). Charge exchange is dominant below 40keV/amu and ion impact ionization above 40keV/amu. Since Janev and Smith's review on atomic data for fusion plasmas in 1993 [21], there has been remarkable progress in theory concerning these cross sections. The newly published charge exchange cross sections appear to be consistent with the recommended data, but discrepancies have been published for ionization in the intermediate energy region (30-150keV/amu). In figure 4(a) the ion impact ionization cross sections from several authors [29, 30, 31, 32] are plotted in comparison with the recommended data [21]. This new data lies higher by about 30% at the peak in the cross section. The Janev and Smith 1993 [21] parametrization at the cross section peak is mostly fitted to the experimental data from Shah et al. [33, 34]. Initially this agreed with close coupling theory, but it was later shown that these results were not converged [31]. Figure 4(b) shows the effect if these increased cross sections would be implemented in the CR beam model. The beam stopping cross section is enhanced by approximately 10% for a typical positive ion source neutral beam operating at 50keV/amu. Until confirmation of these theoretical results, we have in this publication used the recommended fundamental cross sections for beam stopping for the comparison between measured neutral beam densities from beam emission and modelled beam densities. We have also found no experimental evidence in our data that the current beam stopping cross sections would be too low. Note that this issue does not affect the beam emission rates, it only affects the attenuation of the beam in the modelled beam density that is used as comparison. For JET (50keV/amu) the beam density at the magnetic axis would typically be lowered by 15%, this effect increases to 50% for the ITER diagnostic beam (100keV/amu).

2.4. COLLISIONAL-RADIATIVE MODELS FOR THE NEUTRAL BEAM (NKM-RESOLVED)

In the models described above a statistical population among the Stark states within the same n-shell was assumed. The violation of this assumption has clearly been demonstrated on JET [9] and it affects the MSE line ratios and σ/π intensity ratio. Boileau et al. [8] included all parabolic states into the ADAS CR model up to n=4, extending the model with statistically populated levels at higher n. Excitation cross sections between parabolic states (derived from (nlm)-resolved cross sections) are not available in literature and therefore these cross section were calculated in the first Born approximation (B1). Gu et al. [35] repeated this modelling up to n = 5 for use in MSE diagnostic modelling, but their B1 cross sections deviate from those calculated by Boileau et al.. The validity of B1 cross sections at the intermediate beam energies (Section 150keV/amu) used in current experiments is questionable (see e.g. [36, p.258]). Marchuk et al. [4] have calculated the (de)excitation cross sections between all parabolic states in eikonal approximation up to n = 10 and implemented these in the NOMAD CR code [37]. For ionization and charge exchange, no (km)-dependence of the donor atom is assumed and the recommended data [21, with corrected ionization] has been used.

The results show a significant deviation of the Stark line ratios with regard to the statistical expectation. A strong dependence on the angle between the direction of the collisions and the electric field is found. In figure 5(a) the line ratios within the MSE mulitplet are plotted for the three published Stark resolved CR models [8, 35, 4]. Figure 5(b) show the total Balmer-emission rate compared to the same model enforcing a statistical population (restricted to $n = 5$, $T_e = T_i = 5keV$ and beam voltage is 55keV/amu). The difference is small at the densities used in current tokamak experiments. The time the beam needs to reach a steady-state population with regard to the ground state is not significantly altered compared to the model that assumes a statistical population (max. 3cm at 50keV/amu for $n = 3$). The MSE line ratios and =Section 1 intensity ratio will be compared with data from JET in section 4.

3. MEASURED VS. PREDICTED BEAM EMISSION INTENSITY

3.1. CONSISTENCY OF D_α AND D_β BEAM EMISSION INTENSITIES

Beam emission spectra on JET can be recorded along the Lines Of Sight (L.O.S) of the core CXRS diagnostic [38] on either the blue or red shifted wing of the unshifted D_α peak, depending on which viewing geometry is used. In figure 6 a D_α beam emission spectrum is shown and Fig. 7 shows a D_β spectrum. The beam emission features of several beams sometimes overlap and can only be distinguished if either the beam voltage is different or if beams from different beam banks ('normal' or 'tangential' [15]) are used. The spectra shown here originate from a pulse where only one beam effectively contributed. A fitting code has been developed to process the full D_α or D_β spectrum, including the beam driven DI charge exchange contribution and the parasitic CII Zeeman multiplet around 6580Å. The results of the fit are also shown in Figs.6-7. The ion temperature and plasma rotation derived from the DI CX components is in reasonable agreement with the ion temperature and rotation measured on CVI CX, although no extensive comparison has been made.

In order to compare the measured beam emission intensities with the expected beam densities, the NB attenuation code CHEAP (CHarge Exchange Analysis Package) has been used. The measured beam intensities are converted to the local beam densities integrated along a L.O.S using the ADAS10 effective emission rates, and the same quantity is obtained from CHEAP using the known intersections between the L.O.S and the NB. In Fig.8, timetraces of the line integrated NB density (full energy fraction) are shown from both beam emission and from the NB attenuation code. Fig.9(a) shows a radial profile of the NB density for all three energy fractions in the beam. The measured (labelled 'BES') and expected beam densities (labelled 'BMS') show qualitatively the same behaviour, but they differ by a constant factor. There is a larger deviation on the track closest to the edge. This latter observation was also made by Mandl et al. [9] and Boileau et al. [8]. This deviation increases at lower electron density and could qualitatively be attributed to the inappropiate use of steady state emission rates in this region of the plasma where a large electron density gradient exists. We have applied time dependent CR modelling but this did not entirely explain the observations, unless an inaccuracy in the localisation of the measurement or the local electron density was assumed as well.

A comparison of the beam densities measured on D_α and D_β BES respectively, yields an accurate check on the modelled n = 4 to n = 3 population in the beam. The D_β emission rate is approximately a factor 10 lower than the D_α emission rate. Nevertheless, the measured beam densities agree very well using the ADAS10 emission rates. This is illustrated in Fig.9(b) on two consecutive, nearly identical shots, once with the spectrometer tuned to D_α BES, once to D_β. The measured densities agree within approx. 10%, most of the difference is correlated with noise on the LIDAR electron density profile. Note that a relatively large discrepancy was found using the outdated emission rates.

As mentioned before, the BES and CHEAP line integrated beam densities agree very well except for a general scaling factor. In Fig.10 the measured beam density is plotted against the modelled density for the full energy component in the NB. The measured beam density is 34% lower than expected for beam 8.7 [15]. Apart from the issues related to the atomic modelling of the excited states addressed in this paper, this remaining discrepancy could also be due to inaccuracies in the assessment of the intensity calibration and the geometry between L.O.S. and NB.

The calibration and alignment with the beams is described in detail by Giroud et al. [15]. The optics are calibrated with an absolutely calibrated source, except for the last window which is calibrated by sending a laser to a retro reflector inside the tokamak vessel. The alignment between the lines of sight and the neutral beams is based on beam emission Doppler shifts and relative CX intensities when individual beams are switched on/off. The anticipated accuracy of the calibration factor is 6-20% (see [15] for details). The uncertainty on the active volume is as low as 2% [15], but only if the neutral beam path can be assumed to be perfectly characterized. The model used to obtain the path length through the beam assumes a diverging gaussian beam, which is a fair approximation far enough from the beam source. The position and divergence are monitored by the beam footprint on a calorimeter plate in the neutral beam box [39].

The attenuation of the neutral beam and hence the NB power deposition is mainly a function of electron density. The ratio between expected and measured beam densities along a core track as function of integrated electron density along the neutral beam path gives a calibration independent verification of the beam stopping. Within the range of electron densities for which we have beam emission data, we have seen no trend in the ratio of BES to CHEAP full energy beam densities as function of electron density. This gives confidence in the effective beam stopping cross sections that are currently in use, although the range of attenuation factors obtained on a single core track was too small to resolve the issue concerning H(1s) ionization by proton impact mentioned in section 2.3.

3.2. NEUTRAL BEAM POWER FRACTIONS FROM BEAM EMISSION

Following the methodology of section 3.1, beam in plasma emission can be used to characterize the distribution of the beam power over the partial energy fractions in the beam (see e.Fig. Mandl et al. [9] for an earlier application of this method). The results of this analysis have been compared with the power fractions based on measurements on the JET Neutral Beam Test Bed and measured by beam into gas emission ring the neutral beam into the tokamak vessel filled with D_2 gas at low pressure. The JET NB Test Bed does not have a bending magnet to remove ions from the

partially neutralised beam leaving the neutraliser and therefore the test bed analysis is based on the interpretation of beam emission from a mixed beam of ions and neutrals fired onto a gas target. It requires extensive modelling [40, 41] to interpret the spectroscopic data from the test bed in terms of the power fractions in the ion beam leaving the source. This is then modelled forward in order to obtain the power fractions in the neutralized beam. The comparison with the beam in plasma power fractions revealed a misinterpretation of the spectroscopic data on the NB Test Bed as it is described in [40] and [41] (the beam density in eq. (2) in [41] should be beam particle flux, therefore the power in the E/2 and E/3 fractions were underestimated by $\sqrt{2}$ and $\sqrt{3}$ respectively). This error has been corrected and the result of the comparison with beam in plasma emission is shown in Fig.11(a) for a beam voltage scan. Fig. 11(b) shows the comparison for a series of beam into gas discharges on JET. After correction of the test bed power fractions and the beam emission rates, all three methods agree rather well.

For the beam into gas discharges of figure 11(b), the agreement at the highest and lowest voltage is very good, but a slight discrepancy is seen between 40 and 50kV/amu. Experimentally determined H_α emission cross sections from Williams et al. [42] have been used for both the NB into gas power fractions shown here and for the test bed analysis where the emission originates from both the excitation of the neutrals and charge exchange of the ions. The excitation cross sections of atomic hydrogen in H_2 have larger error bars than the H^+ charge exchange cross sections in H_2 [42]. This puts in doubt the reliability of NB into gas experiments for measurement of the NB species mix, despite the more extensive modelling that is required when the power fractions are measured on the ion beam on the test bed or on the neutral beam during standard tokamak operation. The good agreement which is obtained here between the NB in plasma power fractions and the test bed data gives does not only gives some confidence in the voltage scaling of the emission rates between 10 and 55keV/amu, it also indicates that beam into plasma emission is a reliable method to obtain the NB species mix in situ.

4. RELATIVE INTENSITIES WITHIN THE MSE MULTIPLET

The MSE multiplet on JET is sufficiently resolved on the core channels of the CXRS diagnostic to observe the individual lines of the full energy component. Therefore the measured line intensities can be used to check the modelled Stark level population within $n = 3$. Because the -lines are polarized perpendicular to the Lorenz field and the π-line parallel, the observed intensities between $-\sigma$ and π-lines can be distorted if the front end optics are sensitive to the polarization. Therefore only the ratio of the lines within one polarization group provides a direct comparison which is free from geometric or diagnostic artifacts. Figure 12 shows the measured and predicted MSE line ratios in function of electron density. Although the minimum electron density that was obtained, is not low enough to do an accurate check on the electron density scaling, the agreement with the modelled line ratios that were obtained with Marchuk et al.'s CR model [4] is very good and the deviation with the statistical line ratios is clear.

The use of the ratio between the observed σ and π radiance to obtain information on the direction of the Lorenz field, and hence on the magnetic pitch angle, has rarely been successful. This is mainly due to the non-statistical features in the MSE spectrum. The classical polarization based MSE diagnostic [43] is much less sensitive to this effect, except when σ and π lines overlap in the sampled wavelength region. In this case a change in electron density could change the amount of σ and π light which is sampled. In Fig.13 the modelled total σ and π-emissivity is plotted in function of electron density for a beam energy of 55keV/amu. The difference with the statistically expected ratio can be as high as 20% for standard tokamak conditions. In order to compare with the experimentally observed ratio, the disturbing effect of the geometry and the polarization sensitivity of the first mirror was obtained using the ratio between the σ 1- and π3-lines. These originate from the same upper level and hence $\Phi_{\sigma 1}/\Phi_{\pi 3}$ is independent of the population structure. However, because the Stark splitting is usually not large enough, it is in practical situations difficult to obtain this ratio with the accuracy that is needed for direct use as a constraint on the magnetic field reconstruction. The measurements compare well to the model, but the use of $\Phi_{\sigma 1}$ and $\Phi_{\pi 3}$ induces considerable statistical noise.

In Fig. 14, the expected measurement $\Phi_{\sigma 1}/\Phi_{\pi 3}$ is plotted in function of the angle between a line of sight and the Lorentz field taking into account the effects of the n = 3 non-statistical population and a first mirror with an s-reflectivity which is 15% larger than the p-reflectivity. This value was obtained from the $\Phi_{\sigma 1}/\Phi_{\pi 3}$ ratio and the known beam and l.o.s. geometry during a beam into gas shot for which the magnetic field is purely toroidal. One can see that the main effect that causes a deviation between the simple geometrical prediction ($\Phi_\sigma / \Phi_\pi = (1 + \cos^2\theta) / \sin^2\theta$) and the measurements is the non-statistical character of the n = 3 population. The measured points agree very well to the modelled curves, however for the equatorial viewing geometry used here, this method cannot be used to obtain useful information about θ (and hence the magnetic pitch angle), because a large change in θ is needed to cause a measurable change in Φ_σ / Φ_π.

CONCLUSIONS

In this paper we have analysed the consistency of several collisional-radiative models [1, 2, 3] that have been developed to calculate the neutral beam stopping and population of excited states in hydrogen plasmas. The results of the calculations are compared with experimental data from JET. Revisiting the proton impact ionization of excited states and identification of a mistake in the ADAS rescaling of the charge exchange cross sections allowed us to achieve consistency between all models. The corrected data will be in a next ADAS release. The calculated relative n = 3 to n = 4 population agrees within 10% to the measured ratio from JET using the H_α to H_β beam emission intensities. Good agreement is found as well on the power fractions measured with BES and on the JET Neutral Beam Test Bed, if a correction to the analysis in [40, 41] is taken into account. The power fractions measured with neutral beam in gas emission show a sligthly larger deviation. The radial profiles and time traces of the measured and modelled NB density agree well but the overall intensity of the measured beam density is ≈30% lower. The reason for this is uncertain, but could also be due to a combination of calibration, characterization of the beam and alignment between

line of sight and neutral beam rather than due to the atomic data itself. Many of these issues are currently the main motivation to use beam emission. The Stark line intensities within the MSE multiplet are in good agreement with a sublevel resolved model [4]. The measured σ/π intensity is disturbed by the polarization characteristics of the tokamak side optics and the $n = 3$ sub population structure, the latter effect is consistent with the CR modelling.

The overall agreement found on JET between the modelled and expected beam emission intensities gives confidence in the proposed scheme combining charge exchange and beam emission that will be used to measure the helium ash on ITER. The agreement between the modelled and measured MSE spectra gives confidence in the Stark resolved CR modelling and hence such a model could be used to correct the measured σ/π-ratio when used to constrain magnetic field reconstructions.

ACKNOWLEDGEMENT

This work was supported by EURATOM and carried out within the framework of the European Fusion Development Agreement. The views and opinions expressed herein do not necessarily reflect those of the European Commission.

REFERENCES

[1]. H. Anderson, M. Fig von Hellermann, R. Hoekstra, L.D. Horton, A.C. Howman, R.W.Fit. Konig, R. Martin, R.E. Olson, and H.P. Summers. Plasma Physics and Controlled Fusion, **42**:781{806, 2000.

[2]. I.H. Hutchinson. Plasma Physics and Controlled Fusion, **44**(1):71{82, 2002.

[3]. O. Marchuk, Fig. Bertschinger, W. Biel, E. Delabie, M. Fig. von Hellermann, R. Jaspers, and D. Reiter. Review of Scientific Instruments, **79**(10):10F532, 2008.

[4]. O. Marchuk, Yu Ralchenko, R.K. Janev, W. Biel, E. Delabie, and A.M. Urnov. Journal of Physics B-Atomic Mololecular and Optical Physics, **43**(1):011002, 2010.

[5]. R.K. Janev, C.D. Boley, and D.E. Post. Nuclear Fusion, **29**:2125{2140, 1989.

[6]. S. Suzuki, Fit. Shirai, M. Nemoto, K. Tobita, H. Kubo, Fit. Sugie, A. Sakasai, and Y. Kusama. Plasma Physics and Controlled Fusion, **40**(12):2097{2111, 1998.

[7]. R.P. Seraydarian, K.H. Burrell, and R.J. Groebner. Review of Scientific Instruments, **59**(8):1530{1532, 1988.

[8]. A. Boileau, M. Von Hellermann, L.D. Horton, J. Spence, and H.P. Summers., Plasma Physics and Controlled Fusionn, **31**(5):779{804, 1989.

[9]. W. Mandl, R.C. Wolf, M.Fig von Hellermann, and H.P .Summers. Plasma Physics and Controlled Fusion, **35**:1373{1394, 1993.

[10]. M.Fig. von Hellermann, R.J.E. Jaspers, H.P. Summers, and K-D Zastrow. Advanced diagnostics for magnetic and inertial fusion. edited by P Stott et al., Kluwer Academic, N.Y., 125-128, 2001.

[11]. M.De Bock, K. Jakubowska, M.Fig. von Hellermann, R.J.E. Jaspers, A.J.H. Donne, and L. Shmaenok. Review of Scientific Instruments, **75**:4155{4157, 2004.

[12]. R. J. E. Jaspers, M. Fig. von Hellermann, E. Delabie, W. Biel, O. Marchuk, and L. Yao. Review of Scientific Instruments, **79**(10):10F526, 2008.

[13]. W.L. Rowan, M.B. Sampsell, and R.S. Granetz. Review of Scientific Instruments, **75**:3487{3489, 2004.
[14]. H Euringer and Ph Verplancke. Review of Scientific Instruments, **65**:2996{2999, 1994.
[15]. C. Giroud, A.Fig. Meigs, C.R. Negus, K.D. Zastrow, T.M. Biewer, Fit.W. Versloot, and JET-EFDA Contributors. Review of Scientific Instruments, **79**(10):10F525, 2008.
[16]. K. Jakubowska, M.De Bock, R Jaspers, M.Fig. Von Hellermann, and L Shmaenok. Review of Scientific Instruments, **75**(10):3475{3477, 2004.
[17]. N.A. Pablant, K.H. Burrell, R.J. Groebner, D.H. Kaplan, and C.Fit. Holcomb. Review of Scientific Instruments, **79**(10):10F517, 2008.
[18]. R.C. Wolf, L-G Eriksson, M.Fig. Von Hellermann, R. Konig, W. Mandl, and F. Porcelli. Nuclear Fusion, **33**(12):1835, 1993.
[19]. E.L. Foley, F.M. Levinton, H.Y. Yuh, and L.E. Zakharov. Review of Scientific Instruments, **79**(10), 2008.
[20]. C.D. Boley, R.K. Janev, and D.E. Post. Physics Review Letters, **52**(7):534{537, 1984.
[21]. R.K. Janev and J. Smith. Atomic Plasma Materials Int. Data Fusion, 1993.
[22]. P.D. Fainstein, V.H. Ponce, and R.D. Rivarola., Journal of Physics B-Atomic Mololecular and Optical Physics, **23**(9):1481{1489, 1990.
[23]. A. Igarashi and Fit. Shirai. Physical Review A, **50**(6, Part A):4945{4950, 1994.
[24]. M. McCartney and D.S.F Crothers. Zeitschrift fur Physik D-Atoms Molecules and Clusters, **35**(1):1{2, 1995.
[25]. Fig.H. Olivera, R.D. Rivarola, and P.D. Fainstein. Physical Review A, **51**(1):847{849, 1995.
[26]. ALADDIN database maintained by the IAEA. http://www-amdis.iaea.org/aladdin.
[27]. M. O'Mullane. http://www.adas.ac.uk/notes/adas c09-01.pdf.
[28]. H.P. Summers. The ADAS User Manual, version 2.6, http://adas.phys.strath.ac.uk. 2004.
[29]. E.Y. Sidky and C.D. Lin. Physical Review A, **65**(1):012711, 2001.
[30]. A. Kolakowska, M.S. Pindzola, and D. R. Schultz. Physical Review A, **59**(5):3588{3591, 1999.
[31]. Nobuyuki Toshima. Physical Review A, **59**(3):1981{1987, 1999.
[32]. Thomas Fig. Winter. Physical Review A, **80**(3):032701, 2009.
[33]. M.B. Shah and H.B Gilbody. Journal of Physics B-Atomic Mololecular and Optical Physics, **14**(14):2361{2377, 1981.
[34]. M.B. Shah, D.S. Elliott, and H.B. Gilbody. Journal of Physics B-Atomic Mololecular and Optical Physics, **20**(11):2481{2485, 1987.
[35]. M.F. Gu, C.Fit. Holcomb, R.J. Jayakuma, and S.L. Allen. Journal of Physics B-Atomic Mololecular and Optical Physics, **41**(9):095701, 2008.
[36]. B.H. Bransden and McDowell M.R.C. Charge Exchange and the Theory of Ion-Atom Collisions. Clarendon Press, Oxford, 1992.
[37]. Yu Ralchenko and Y Maron. Journal of Quantitative Spectroscopy Radiative Transfer, **71**(2-6):609{621, 2001.
[38]. C.R. Negus, C. Giroud, A.Fig. Meigs, K.D. Zastrow, D.L. Hillis, and JET-EFDA Contributors. Review of Scientific Instruments, **77**(10):10F102, 2006.

[39]. D. Ciric, J.J. Milnes, and E. Surrey. Misalignment on multi-aperture particle beam properties. 19th IEEE/NPSS Symposium on Fusion Engineering, 2002.

[40]. R.S. Hemsworth. JET-DN-C(85)**8**, 1985.

[41]. R. Uhlemann, R.S. Hemsworth, Fig. Wang, and H. Euringer. Review of Scientific Instruments, **64**:974{982, 1993.

[42]. I.D. Williams, J. Geddes, and H.B. Gilbody. Journal of Physics B-Atomic Mololecular and Optical Physics, **15**:1377{1389, 1982.

[43]. F.M. Levinton, R.J. Fonck, Fig.M. Gammel, R. Kaita, H.W. KugelL, ET Powell, and DW Roberts. Physics Review Letters, **63**(19):2060{2063, 1989.

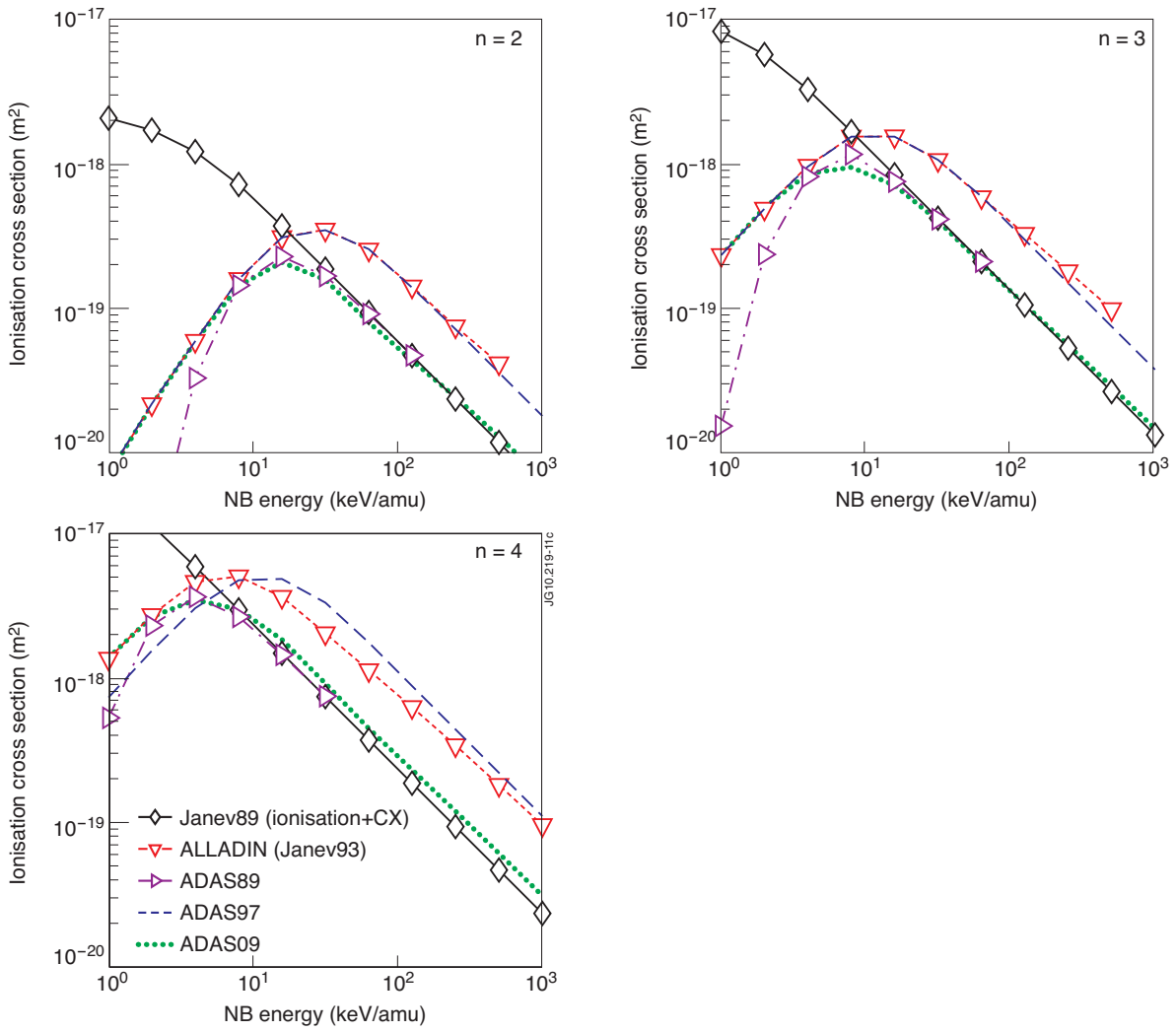

Figure 1: Proton impact ionization of excited states of the hydrogen atom. Recommended data sets (Janev89 [5] and Janev93 (as in the ALLADIN database) [21, 26]) and data used in the ADAS beam emission models are shown.

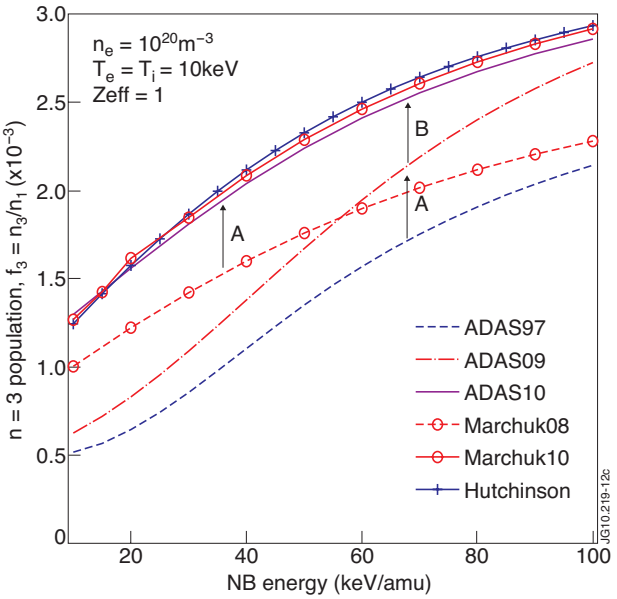

*Figure 2: n = 3 population in the beam with regard to the ground state according to dierent CR models. ADAS: ADAS excited beam population [1, 28]; Marchuk: n = 3 population from Marchuk et al.[3]; Hutchinson: excited population digitised from Fig.3 in Hutchinson [2]. **A** denotes the change due to the correction of H(n>1) ionization, **B** marks the change due to a correction of H(n>1) charge exchange in ADAS.*

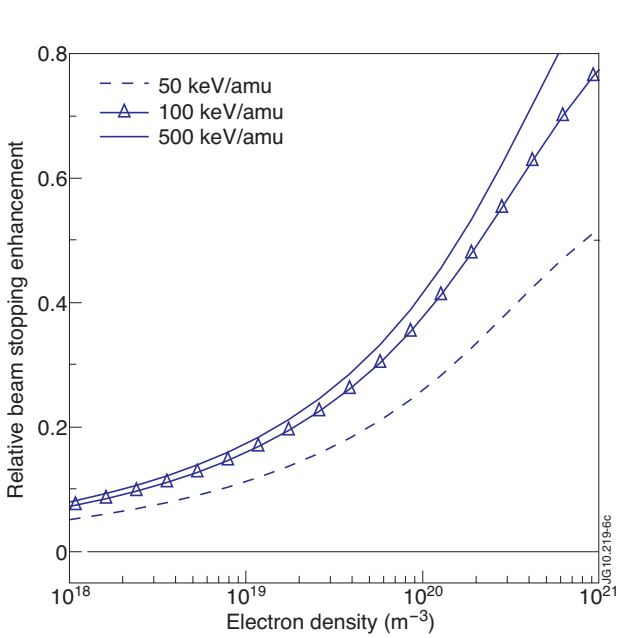

(a) Relative increase of the beam stopping cross section due to stepwise ionization trough excited states in function of electron density, using the CR model of Marchuk et al. [3]. ($T_e = T_i = 5keV$, $Z_{eff} = 1$)

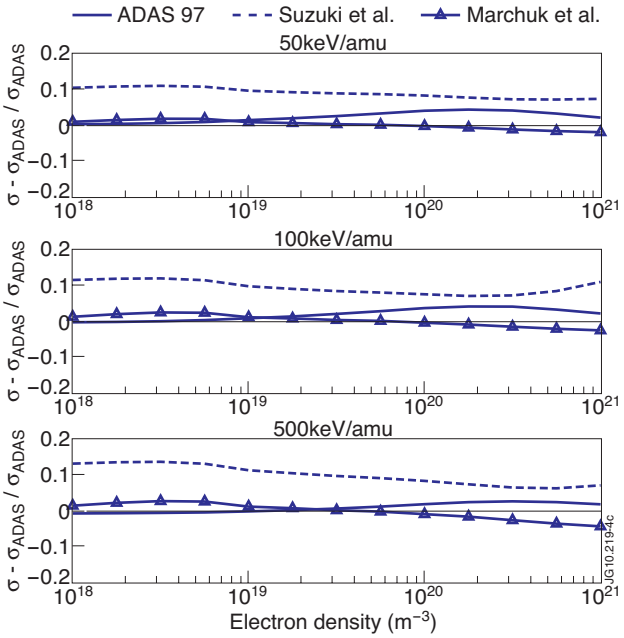

(b) Comparison of NB stopping cross sections from several CR models for the NB. The difference due to the correction of the excited state ionization and charge exchange is also shown. ($T_e = T_i = 5keV$, $Z_{eff} = 1$)

Figure 3: The role of excited states in NB stopping and consistency of beam stopping cross sections from several models.

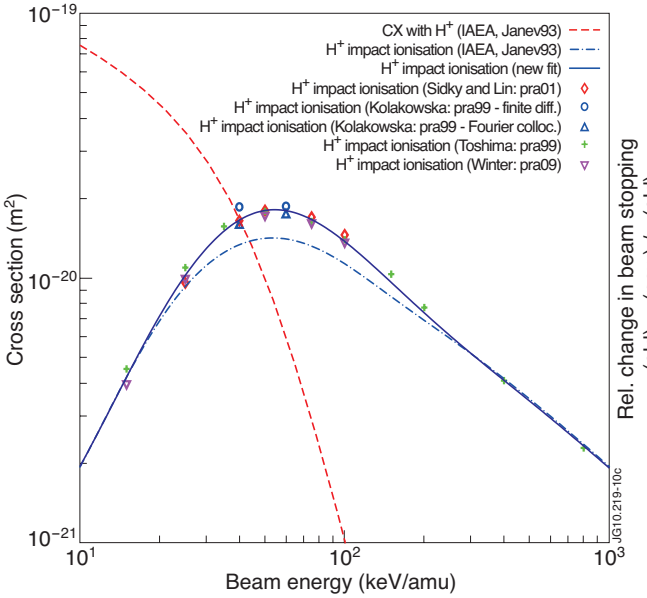

(a) Recommended data for ionization and charge exchange compared with data from recent theoretical publications [29, 30, 31, 32].

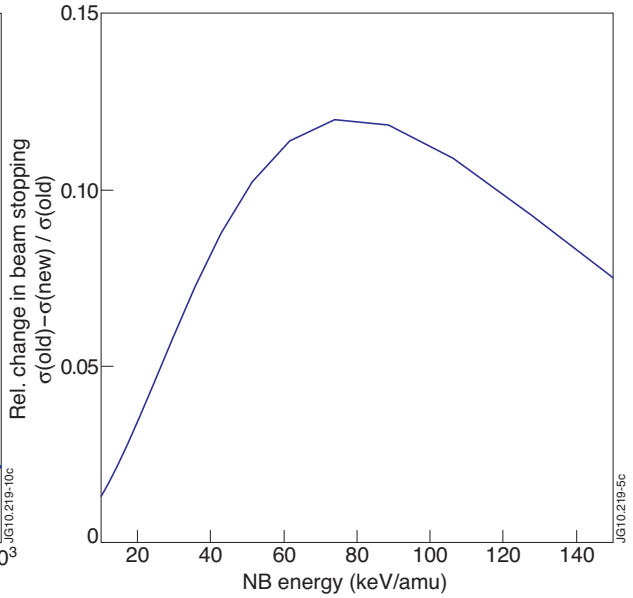

(b) Impact of the change in ion impact ionization on the NB stopping cross section. ($T_e = T_i = 5keV$, $Z_{eff} = 1$)

Figure 4: Recent theoretical results on the cross sections for H^+ impact ionization and charge exchange of H(1s), and the impact on the effective beam stopping cross sections.

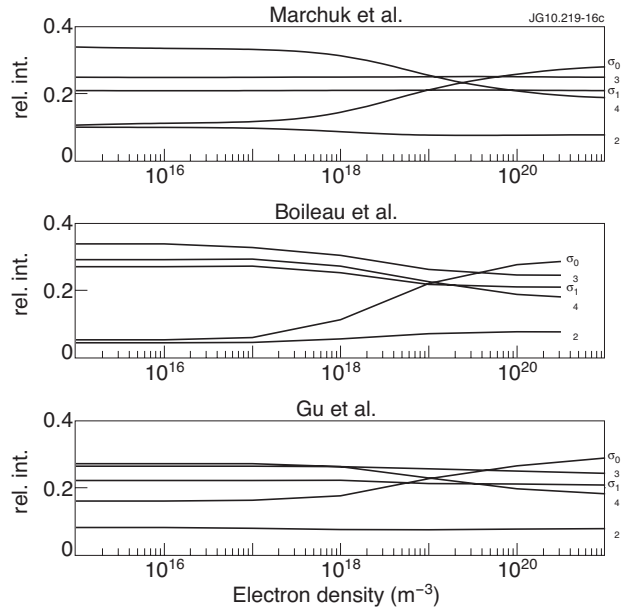

(a) Line ratios within the MSE mulitplet from several Stark resolved CR models [4, 8, 35].

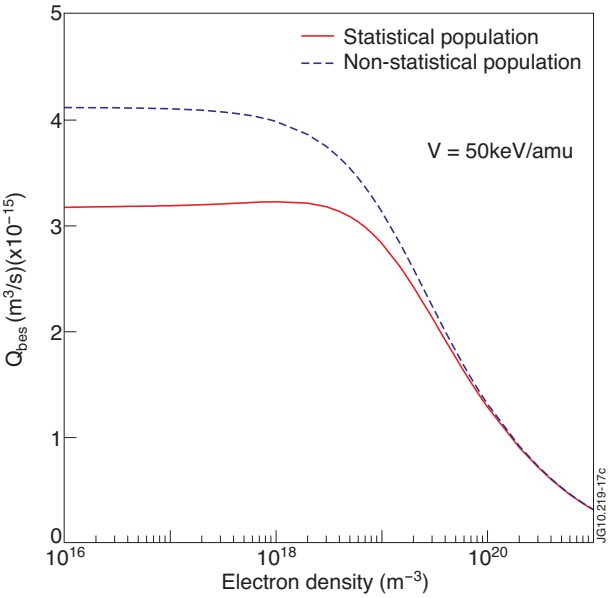

(b) Comparison of the H beam emission rate for the (nkm)- and n-resolved CR model of Marchuk et al. [4] (restricted to n = 5, V = 55keV/amu,$T_e = T_i = 5keV$)

Figure 5: Effect of Stark level resolved modelling on the MSE line ratios and on the total H_α beam emission rate.

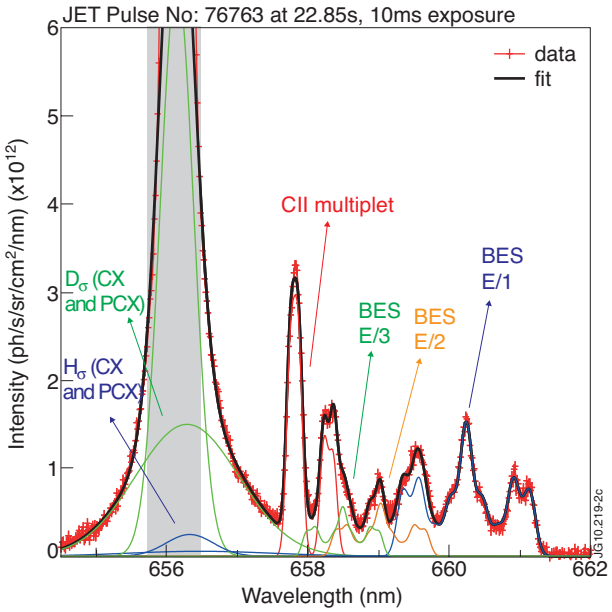

Figure 6: D_α spectrum from JET, the experimental data is in red, other lines are fitted features. The three energy components of the BES spectrum are indicated. The active and passive D/H CX contributions are approximated as gaussian lines. The coldest part of the D/H spectrum (the grey area) is usually overexposed and is neglected in the fit.

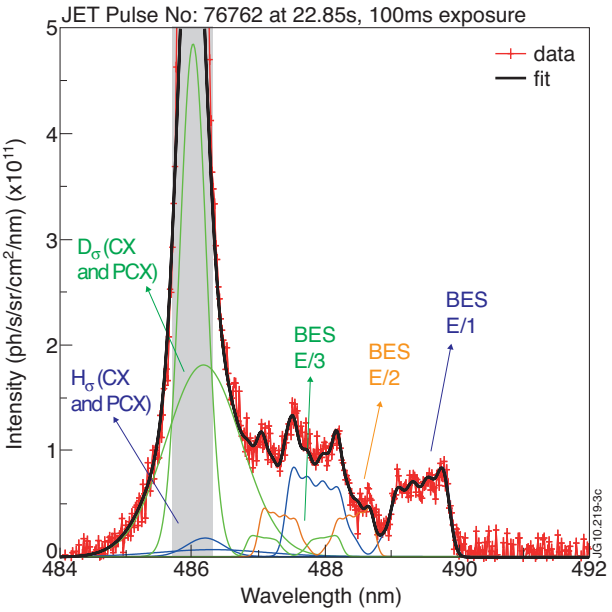

Figure 7: Example D_β spectrum from JET. The coldest part of the D/H spectrum (the grey area) is neglected in the fit.

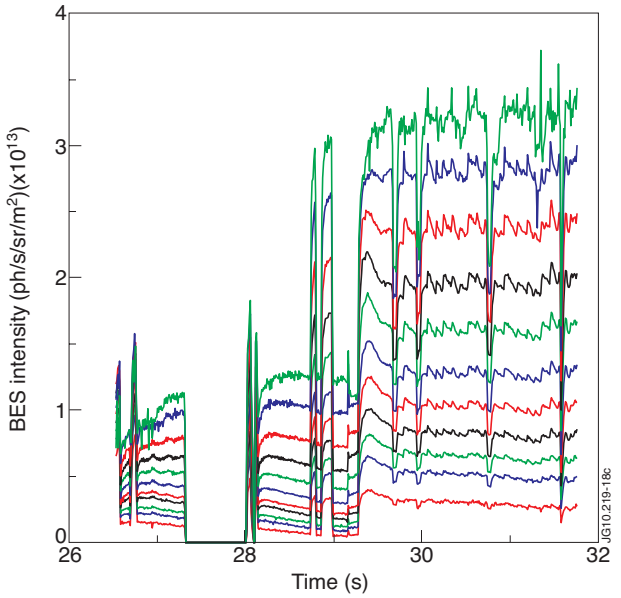

a) Beam emission intensity of the full energy component for Pulse No: 72324 along several lines of sight of the JET core CXRS diagnostic. Two beams contribute to the beam emission spectrum.

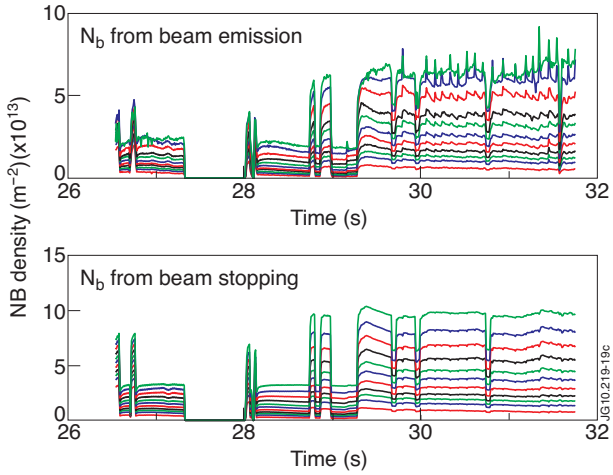

(b) Time traces of the line integrated NB density (E/1 component) derived from beam emission (top) and from a NB attenuation code (bottom) for Pulse No: 72324. Two beams contribute to the line integrated beam density.

Figure 8: Time traces of the beam emission intensity and the beam density along a line of sight (E/1 component beam 8.7 + 8.8).

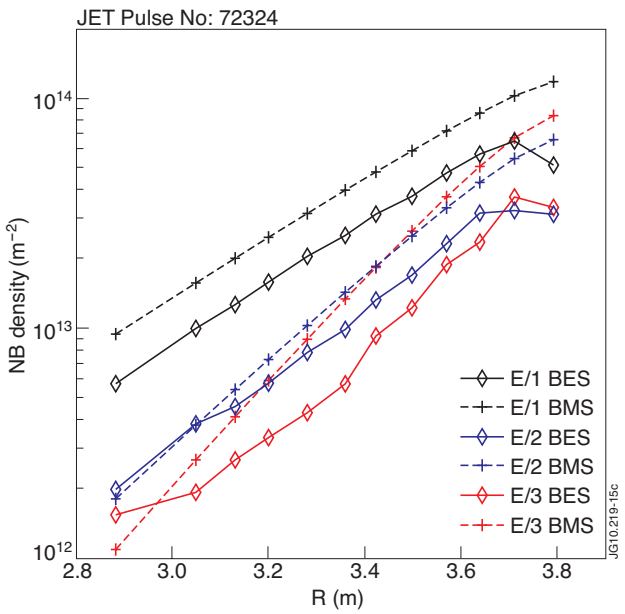

(a) Profile of the NB density integrated along a L.O.S for the three energy fractions in the beam for Pulse No: 72324 at 30.3s. 'BES' refers to measured data using beam emission, 'BMS' is the expectation from a beam stopping code.

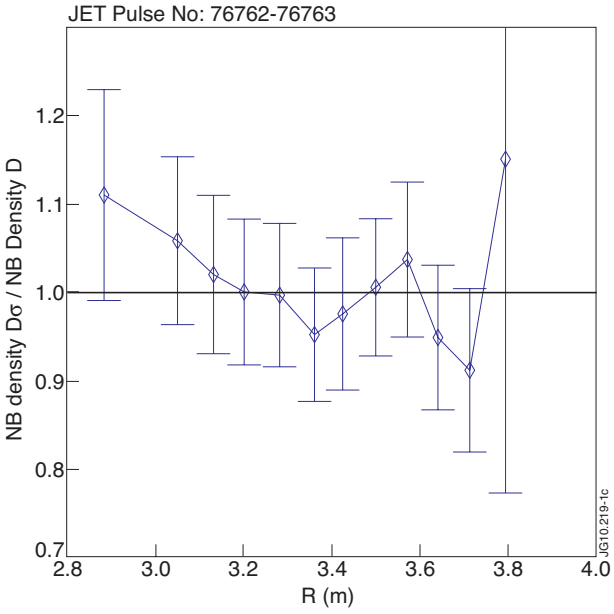

(b) Ratio of NB densities measured on D_α and D_β beam emission from two similar discharges. The NB attenuation code predicts a maximum dierence between the shots of approximately 5% at this time frame. The beam density measured on D_α is consistent with the beam density measured on D_β.

Figure 9: Consistency between beam densities from beam emission and the expected NB density from a beam attenuation code (Pulse No: 72324) and consistency between D_α and D_β.

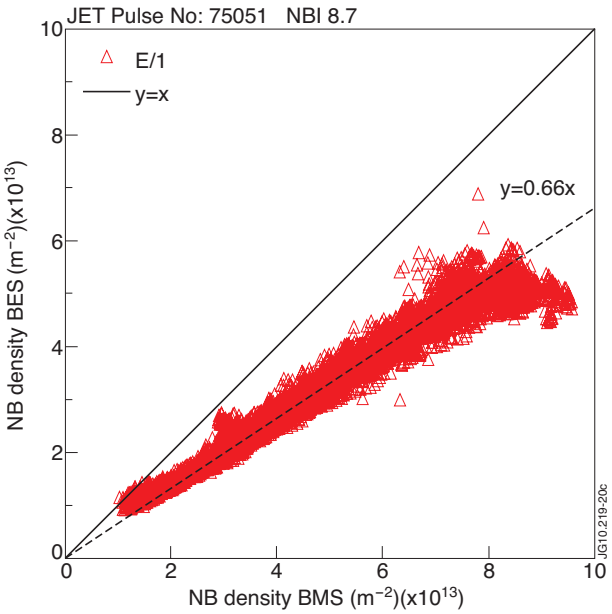

Figure 10: NB density from BES against the beam stopping (BMS) prediction for beam 8.7 (Pulse No: 75051). The odd edge channel is neglected.

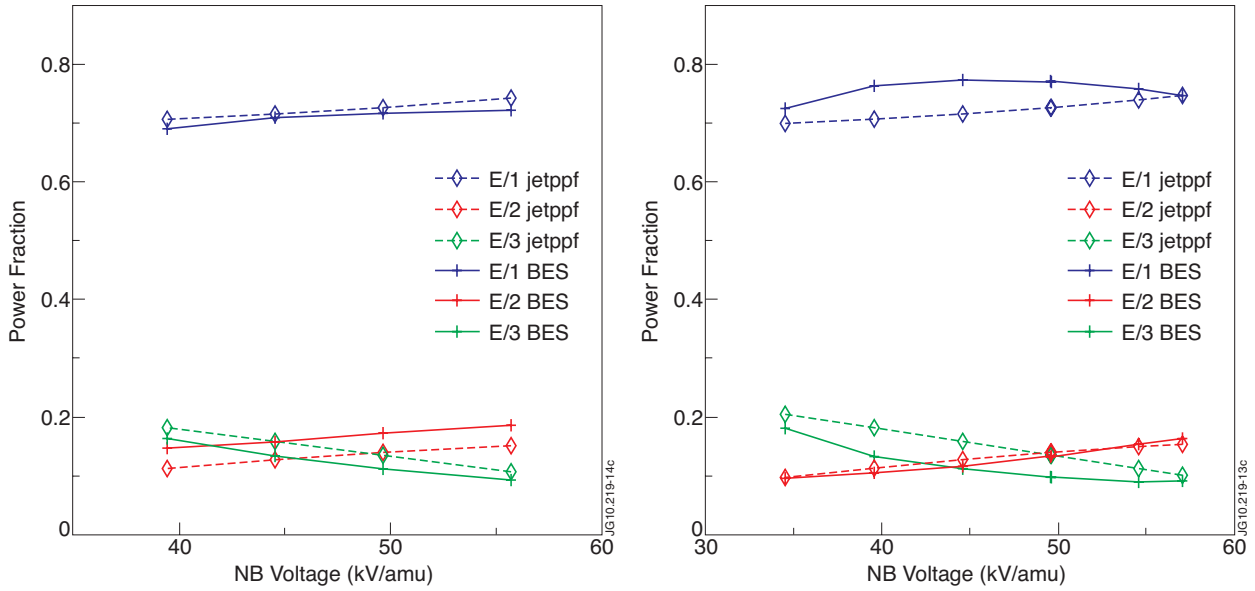

(a) The data labelled 'BES' is from beam emission in plasma (Pulse No's: 75046-75050), the data labelled 'jetppf' shows the expected power fractions.

(b) The data labelled 'BES' is from beam in gas emission (Pulse No's:77528-77534), the data labelled 'jetppf' shows the expected power fractions.

Figure 11: Distribution of the power among the fractional energy components in the NB, in function of beam voltage. The power fractions measured with beam emission are compared with the expected fractions from a model based on test bed measurements.

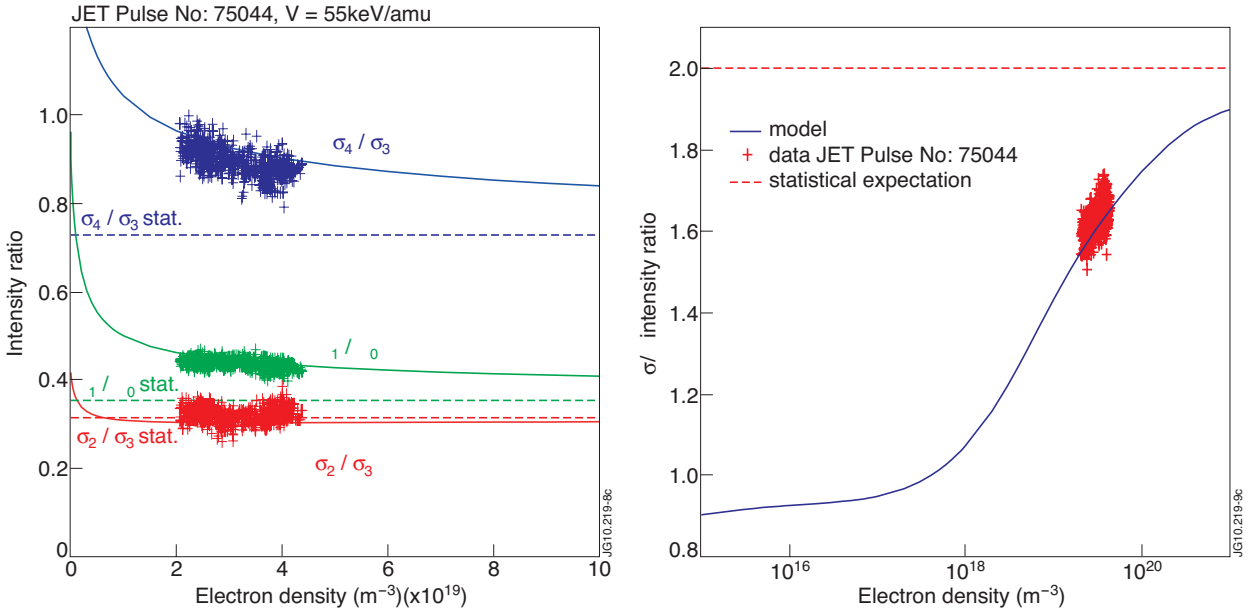

Figure 12: Stark line ratios within the MSE multiplet in function of electron density. Data from a central track of the JET core CXRS diagnostic (MSE multiplet best resolved) is compared with the model from Marchuk et al. [4]. The dashed lines show the expected line ratios when the n = 3 level would have a statistical subpopulation.

Figure 13: Ratio between the total σ- and π-emissivity (integrated over all solid angles). The experimental data points have been obtained from the measured σ- and π-radiances through $\frac{I_\sigma}{I_\pi} = \frac{\Phi_\pi}{\Phi_\pi} \Big/ \frac{\Phi_{\sigma 1} A_{\pi 3}}{\Phi_{\pi 3} A_{\sigma 3}}$ *The label 'model' refers to the model of Marchuk et al. [4]. The dashed line shows the statistical prediction* $I_\sigma = 2I_\pi$.

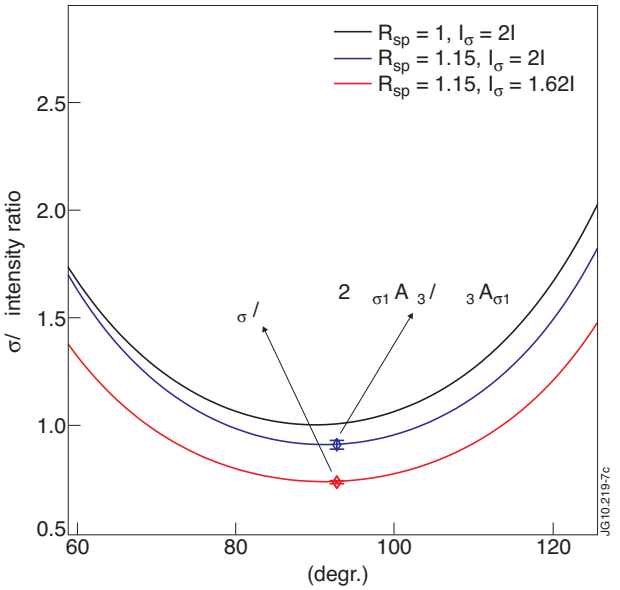

Figure 14: Ratio of the expected σ- over π-radiance in function of angle θ between a core line of sight and the Lorentz field. R_{sp} is the ratio between the s-and p- reflecivity of the first mirror. The case $R_{sp} = 1$, $I_\sigma = 2I_\pi$ corresponds to the standard prediction $\Phi_\sigma / \Phi_\pi = (1 + \cos^2 \theta) / \sin^2 \theta$. The blue and red curve correspond to the situation with a polarization sensitive first mirror and with a n = 3 population that has not reached a statistical distribution. The points indicate measurements from JET Pulse No: 75044. For this viewing geometry a large change in is needed to cause an appreciable change in the measured Φ_σ / Φ_π intensity ratio.

ABSTRACT.
Several Collisional-Radiative (CR) models [1, 2, 3] have been developed to calculate the attenuation and the population of excited states of hydrogen or deuterium beams injected into tokamak plasmas. The datasets generated by these CR models are needed for the modelling of beam ion deposition and (excited) beam densities in current experiments, and the reliability of this data will be crucial to obtain helium ash densities on ITER combining charge exchange and beam emission spectroscopy. Good agreement between the different CR models for the Neutral Beam (NB) is found, if corrections to the fundamental cross sections are taken into account. First the H_α and H_β beam emission spectra from JET are compared with the expected intensities. Second, the line ratios within the Stark multiplet are compared with the predictions of a sublevel resolved model. The measured intensity of the full multiplet is ≈30% lower than expected on the basis of beam attenuation codes and the updated beam emission rates, but apart from the atomic data this could also be due to the characterization of the NB path and line of sight integration and the absolute calibration of the optics. The modelled $n = 3$ to $n = 4$ population agrees very well with the ratio of the measured H_α to H_β beam emission intensities. Good agreement is found as well between the neutral beam power fractions measured with beam emission in plasma and on the JET Neutral Beam Test Bed. The Stark line ratios and σ/π intensity ratio deviate from a statistical distribution, in agreement with the CR model in parabolic states from Marchuk et al. [4].

1. MOTIVATION

Powerful neutral hydrogen or deuterium beams provide the dominant external heating and momentum input in most large scale tokamak experiments. For the interpretation of neutral beam (NB) heated discharges, detailed knowledge is required about the energy distribution of the neutrals (power fractions) and the attenuation of the beams in order to obtain radial proles of the fast ion deposition and hence of the heating, torque and beam driven current. For the quantitative interpretation of Charge eXchange (CX) spectra, the local NB fluxes and population of excited states in the beam are needed to convert CX emissivities into local impurity densities. All these calculations strongly rely on the accuracy of the atomic data for the NB that is provided by Collisional-Radiative (CR) models of the beam [1, 2, 3, 5, 6].

When the Beam Emission Spectrum (BES) was recorded for the first time, it was immediately proposed to monitor the beam attenuation, and hence the accuracy of the effective beam stopping cross sections, by using the observed beam emission intensities [7, 8]. This replaces the accumulated error on the beam attenuation along the beam path [9], by a local error in the beam emission rate. Beam emission, when combined with Charge eXchange Recombination Spectroscopy (CXRS), also has the potential of reducing the need of an absolute calibration of the CXRS spectra and a calculation of the intersection integral between a line of sight and the NB, to a relative calibration between several spectral bands [8, 10, 11]. The combination of BES and CXRS is the only feasible method to measure helium ash concentrations with the requested accuracy on ITER where only a small fraction (≈1%) of the diagnostic beam reaches the plasma center and where calibrations of

the tokamak side optics on a regular basis will be impossible [12]. The beam emission intensity and Doppler shift is also widely used to characterise the beam (power fractions [9, 13, 14], alignment [15], divergence [14]).

Apart from using the intensity of the full BES multiplet, the σ/π intensity ratio [9, 16, 17, 12] and Stark splitting [18, 19] can be used as an alternative to polarisation based Motional Stark effect (MSE) diagnostics, as proposed for the ITER diagnostic and heating beam respectively. For these applications the Stark level population structure of the beam neutrals is required to model the spectra, like for polarisation based MSE diagnostics when σ and π-lines overlap.

Despite these promising applications, the use of beam emission has been hampered by the reliability of the involved atomic data and the complexity of the spectra. At the same time, the modelled NB fast ion deposition has been exploited at ever higher accuracy, thereby strongly relying on the accuracy of the underlying beam stopping calculations. It is the aim of this paper to check the consistency of the various beam modelling efforts and to quantitatively compare modelled neutral beam densities with measured beam densities from beam emission on JET.

In section 2 several published CR models for the neutral beam are compared. A distinction is made between models that implicitly assume a statistical population of the Stark levels within an n-shell (section 2.1-2.3) and models that have Stark level resolution (section 2.4). The latter models are mainly useful for the analysis of MSE data. In section 3 measured beam emission intensities from JET are compared to the expected beam densities from the beam stopping calculations. The expected line ratios within the MSE multiplet are compared with experimental data in section 4.

2. ATOMIC MODELS OF THE NEUTRAL BEAM

2.1. COLLISIONAL-RADIATIVE MODELS FOR THE NEUTRAL BEAM (N-RESOLVED)

The first neutral beam models that take excited states into account are by Boley et al. [20] and Janev et al. [5]. The focus of these works was solely on the penetration length of neutral beams. Although beam stopping is mainly determined by direct proton impact ionization and charge exchange from the ground state, excited states become increasingly important with increasing beam energy and plasma density. Seraydarian et al. [7] found relatively good agreement between the measured and predicted beam emission intensity on DIII-D, using a model based on the data of Boley et al. [20]. However, the ion impact excitation cross sections used in [20] were too large, which makes the interpretation of the beam emission results in [7] difficult. Mandl et al. [9] compared the measured and expected beam densities on JET using the ADAS CR model (here referred to as ADAS89). They found relatively good agreement between model and experiment. Anderson et al. [1] thoroughly revisited the ADAS beam model (here referred to as ADAS97) and brought it to a large extent in line with the 1993 review of atomic data by Janev and Smith [21]. The observed intensity on JET was found to be 30% lower than predicted. Hutchinson [2] built a CR model of the beam based on the Janev 1989 and 1993 atomic datasets [5, 21] and found a large discrepancy with ADAS97. Marchuk et al. [3] assessed the atomic data needs for active beam spectroscopy on ITER (based on the Janev 1993 dataset) and found a good agreement between their CR model and ADAS97, but

only compared for the ITER diagnostic beam relevant conditions of 100keV/amu.

2.2. CONSISTENCY OF ATOMIC DATA FOR NB EMISSION

An investigation of the discrepancies between the CR models [1, 2, 3] revealed two issues: (1) The high energy part of the proton impact ionization cross section for excited states published in the Janev 1993 review is based on erroneous input data from [22]. Although this error was noted [23, 24] and corrected by the authors [25], the IAEA recommended data in the Alladin database [26] has not changed yet. A new fit to the ionization cross sections has been made and implemented in the CR models of ADAS (see [27] for details) and Marchuk et al. The different datasets are compared in Fig.1. (2) Furthermore, a bug in the ADAS CR code affected the CX cross sections for excited donor states in hydrogen, strongly affecting the beam emission rates below 100keV/amu. The corrected dataset will here be referred to as ADAS10[1]. The result of these corrections is visually depicted in Fig.2. Both the corrected emission rates of ADAS, Marchuk et al. and Hutchinson agree within 5% for the plasma and beam conditions studied here. The measured beam densities derived from these beam emission rates will be compared with experimental data from JET in section 3.

2.3. CONSISTENCY OF ATOMIC DATA FOR NB STOPPING

The changes mentioned above in the electron loss cross sections from excited states in the neutral beam, and the corresponding uncertainties, have only a small influence on the NB stopping cross sections for current experiments. This is because excited states only contribute ≈20% to the effective beam stopping cross section for JET-like beams and plasmas (50keV/amu, $n_e = 5\times10^{19}$ m^{-3}). For ITER-like beams (500keV/amu, $n_e = 5\times10^{19}$ m^{-3}) however this augments to ≈45%. The models used here do not take ionization by the Lorentz field into account, which is negligible for present experimental conditions but could increase the ionization through excited states even further for the ITER heating beams. In figure 3(a) the increase of the beam stopping cross section due to step wise ionization is shown as a function of electron density for several NB energies. In figure 3(b) beam stopping cross sections from several datasets are compared. The difference between the beam stopping cross sections from ADAS and Marchuk et al. [3] is in all conditions below a few percent. The analytical expressions for the beam stopping cross sections provided by Suzuki et al. [6] are on average 10% higher for current experimental conditions. The 1989 effective beam stopping data from Janev et al. [5], which is based on outdated data compared to the 1993 review by Janev and Smith [21] and is not shown here, is higher by more than 20% but merges with the current data at beam energies of several 100keV/amu. The change between the ADAS10 and ADAS97 beam stopping cross sections is also plotted. The dfference stays below 5%. In conclusion, the different sets of beam stopping data for deuterium plasmas [1, 3, 6] only show a small deviation and are for current experimental conditions dominated by ion impact ionization and charge exchange from the ground state. Changes in the excited population (e.g. Fig. ADAS97 vs. ADAS10) only have a modest impact on beam stopping. It is the accuracy of the fundamental datasets concerning the ground state that determines the overal accuracy of the beam stopping cross sections. The quality

[1] *This data is part of ADAS release v3.1.*

of proton impact ionization from the ground state is classified in category B by the IAEA [26] and charge exchange with low-Z ions is categorised as B-C (B: uncertainty 10-25%, C: 25-50%). Charge exchange is dominant below 40keV/amu and ion impact ionization above 40keV/amu. Since Janev and Smith's review on atomic data for fusion plasmas in 1993 [21], there has been remarkable progress in theory concerning these cross sections. The newly published charge exchange cross sections appear to be consistent with the recommended data, but discrepancies have been published for ionization in the intermediate energy region (30-150keV/amu). In figure 4(a) the ion impact ionization cross sections from several authors [29, 30, 31, 32] are plotted in comparison with the recommended data [21]. This new data lies higher by about 30% at the peak in the cross section. The Janev and Smith 1993 [21] parametrization at the cross section peak is mostly fitted to the experimental data from Shah et al. [33, 34]. Initially this agreed with close coupling theory, but it was later shown that these results were not converged [31]. Figure 4(b) shows the effect if these increased cross sections would be implemented in the CR beam model. The beam stopping cross section is enhanced by approximately 10% for a typical positive ion source neutral beam operating at 50keV/amu. Until confirmation of these theoretical results, we have in this publication used the recommended fundamental cross sections for beam stopping for the comparison between measured neutral beam densities from beam emission and modelled beam densities. We have also found no experimental evidence in our data that the current beam stopping cross sections would be too low. Note that this issue does not affect the beam emission rates, it only affects the attenuation of the beam in the modelled beam density that is used as comparison. For JET (50keV/amu) the beam density at the magnetic axis would typically be lowered by 15%, this effect increases to 50% for the ITER diagnostic beam (100keV/amu).

2.4. COLLISIONAL-RADIATIVE MODELS FOR THE NEUTRAL BEAM (NKM-RESOLVED)

In the models described above a statistical population among the Stark states within the same n-shell was assumed. The violation of this assumption has clearly been demonstrated on JET [9] and it affects the MSE line ratios and σ/π intensity ratio. Boileau et al. [8] included all parabolic states into the ADAS CR model up to n=4, extending the model with statistically populated levels at higher n. Excitation cross sections between parabolic states (derived from (nlm)-resolved cross sections) are not available in literature and therefore these cross section were calculated in the first Born approximation (B1). Gu et al. [35] repeated this modelling up to n = 5 for use in MSE diagnostic modelling, but their B1 cross sections deviate from those calculated by Boileau et al.. The validity of B1 cross sections at the intermediate beam energies (Section 150keV/amu) used in current experiments is questionable (see e.g. [36, p.258]). Marchuk et al. [4] have calculated the (de)excitation cross sections between all parabolic states in eikonal approximation up to n = 10 and implemented these in the NOMAD CR code [37]. For ionization and charge exchange, no (km)-dependence of the donor atom is assumed and the recommended data [21, with corrected ionization] has been used.

The results show a significant deviation of the Stark line ratios with regard to the statistical expectation. A strong dependence on the angle between the direction of the collisions and the electric field is found. In figure 5(a) the line ratios within the MSE mulitplet are plotted for the three published Stark resolved CR models [8, 35, 4]. Figure 5(b) show the total Balmer-emission rate compared to the same model enforcing a statistical population (restricted to $n = 5$, $T_e = T_i = 5keV$ and beam voltage is 55keV/amu). The difference is small at the densities used in current tokamak experiments. The time the beam needs to reach a steady-state population with regard to the ground state is not significantly altered compared to the model that assumes a statistical population (max. 3cm at 50keV/amu for $n = 3$). The MSE line ratios and =Section 1 intensity ratio will be compared with data from JET in section 4.

3. MEASURED VS. PREDICTED BEAM EMISSION INTENSITY

3.1. CONSISTENCY OF D_α AND D_β BEAM EMISSION INTENSITIES

Beam emission spectra on JET can be recorded along the Lines Of Sight (L.O.S) of the core CXRS diagnostic [38] on either the blue or red shifted wing of the unshifted D_α peak, depending on which viewing geometry is used. In figure 6 a D_α beam emission spectrum is shown and Fig. 7 shows a D_β spectrum. The beam emission features of several beams sometimes overlap and can only be distinguished if either the beam voltage is different or if beams from different beam banks ('normal' or 'tangential' [15]) are used. The spectra shown here originate from a pulse where only one beam effectively contributed. A fitting code has been developed to process the full D_α or D_β spectrum, including the beam driven DI charge exchange contribution and the parasitic CII Zeeman multiplet around 6580Å. The results of the fit are also shown in Figs.6-7. The ion temperature and plasma rotation derived from the DI CX components is in reasonable agreement with the ion temperature and rotation measured on CVI CX, although no extensive comparison has been made.

In order to compare the measured beam emission intensities with the expected beam densities, the NB attenuation code CHEAP (CHarge Exchange Analysis Package) has been used. The measured beam intensities are converted to the local beam densities integrated along a L.O.S using the ADAS10 effective emission rates, and the same quantity is obtained from CHEAP using the known intersections between the L.O.S and the NB. In Fig.8, timetraces of the line integrated NB density (full energy fraction) are shown from both beam emission and from the NB attenuation code. Fig.9(a) shows a radial profile of the NB density for all three energy fractions in the beam. The measured (labelled 'BES') and expected beam densities (labelled 'BMS') show qualitatively the same behaviour, but they differ by a constant factor. There is a larger deviation on the track closest to the edge. This latter observation was also made by Mandl et al. [9] and Boileau et al. [8]. This deviation increases at lower electron density and could qualitatively be attributed to the inappropiate use of steady state emission rates in this region of the plasma where a large electron density gradient exists. We have applied time dependent CR modelling but this did not entirely explain the observations, unless an inaccuracy in the localisation of the measurement or the local electron density was assumed as well.

A comparison of the beam densities measured on D_α and D_β BES respectively, yields an accurate check on the modelled n = 4 to n = 3 population in the beam. The D_β emission rate is approximately a factor 10 lower than the D_α emission rate. Nevertheless, the measured beam densities agree very well using the ADAS10 emission rates. This is illustrated in Fig.9(b) on two consecutive, nearly identical shots, once with the spectrometer tuned to D_α BES, once to D_β. The measured densities agree within approx. 10%, most of the difference is correlated with noise on the LIDAR electron density profile. Note that a relatively large discrepancy was found using the outdated emission rates.

As mentioned before, the BES and CHEAP line integrated beam densities agree very well except for a general scaling factor. In Fig.10 the measured beam density is plotted against the modelled density for the full energy component in the NB. The measured beam density is 34% lower than expected for beam 8.7 [15]. Apart from the issues related to the atomic modelling of the excited states addressed in this paper, this remaining discrepancy could also be due to inaccuracies in the assessment of the intensity calibration and the geometry between L.O.S. and NB.

The calibration and alignment with the beams is described in detail by Giroud et al. [15]. The optics are calibrated with an absolutely calibrated source, except for the last window which is calibrated by sending a laser to a retro reflector inside the tokamak vessel. The alignment between the lines of sight and the neutral beams is based on beam emission Doppler shifts and relative CX intensities when individual beams are switched on/off. The anticipated accuracy of the calibration factor is 6-20% (see [15] for details). The uncertainty on the active volume is as low as 2% [15], but only if the neutral beam path can be assumed to be perfectly characterized. The model used to obtain the path length through the beam assumes a diverging gaussian beam, which is a fair approximation far enough from the beam source. The position and divergence are monitored by the beam footprint on a calorimeter plate in the neutral beam box [39].

The attenuation of the neutral beam and hence the NB power deposition is mainly a function of electron density. The ratio between expected and measured beam densities along a core track as function of integrated electron density along the neutral beam path gives a calibration independent verification of the beam stopping. Within the range of electron densities for which we have beam emission data, we have seen no trend in the ratio of BES to CHEAP full energy beam densities as function of electron density. This gives confidence in the effective beam stopping cross sections that are currently in use, although the range of attenuation factors obtained on a single core track was too small to resolve the issue concerning H(1s) ionization by proton impact mentioned in section 2.3.

3.2. NEUTRAL BEAM POWER FRACTIONS FROM BEAM EMISSION

Following the methodology of section 3.1, beam in plasma emission can be used to characterize the distribution of the beam power over the partial energy fractions in the beam (see e.Fig. Mandl et al. [9] for an earlier application of this method). The results of this analysis have been compared with the power fractions based on measurements on the JET Neutral Beam Test Bed and measured by beam into gas emission ring the neutral beam into the tokamak vessel filled with D_2 gas at low pressure. The JET NB Test Bed does not have a bending magnet to remove ions from the

partially neutralised beam leaving the neutraliser and therefore the test bed analysis is based on the interpretation of beam emission from a mixed beam of ions and neutrals fired onto a gas target. It requires extensive modelling [40, 41] to interpret the spectroscopic data from the test bed in terms of the power fractions in the ion beam leaving the source. This is then modelled forward in order to obtain the power fractions in the neutralized beam. The comparison with the beam in plasma power fractions revealed a misinterpretation of the spectroscopic data on the NB Test Bed as it is described in [40] and [41] (the beam density in eq. (2) in [41] should be beam particle flux, therefore the power in the E/2 and E/3 fractions were underestimated by $\sqrt{2}$ and $\sqrt{3}$ respectively). This error has been corrected and the result of the comparison with beam in plasma emission is shown in Fig.11(a) for a beam voltage scan. Fig. 11(b) shows the comparison for a series of beam into gas discharges on JET. After correction of the test bed power fractions and the beam emission rates, all three methods agree rather well.

For the beam into gas discharges of figure 11(b), the agreement at the highest and lowest voltage is very good, but a slight discrepancy is seen between 40 and 50kV/amu. Experimentally determined H_α emission cross sections from Williams et al. [42] have been used for both the NB into gas power fractions shown here and for the test bed analysis where the emission originates from both the excitation of the neutrals and charge exchange of the ions. The excitation cross sections of atomic hydrogen in H_2 have larger error bars than the H^+ charge exchange cross sections in H_2 [42]. This puts in doubt the reliability of NB into gas experiments for measurement of the NB species mix, despite the more extensive modelling that is required when the power fractions are measured on the ion beam on the test bed or on the neutral beam during standard tokamak operation. The good agreement which is obtained here between the NB in plasma power fractions and the test bed data gives does not only gives some confidence in the voltage scaling of the emission rates between 10 and 55keV/amu, it also indicates that beam into plasma emission is a reliable method to obtain the NB species mix in situ.

4. RELATIVE INTENSITIES WITHIN THE MSE MULTIPLET

The MSE multiplet on JET is sufficiently resolved on the core channels of the CXRS diagnostic to observe the individual lines of the full energy component. Therefore the measured line intensities can be used to check the modelled Stark level population within $n = 3$. Because the -lines are polarized perpendicular to the Lorenz field and the π-line parallel, the observed intensities between $-\sigma$ and π-lines can be distorted if the front end optics are sensitive to the polarization. Therefore only the ratio of the lines within one polarization group provides a direct comparison which is free from geometric or diagnostic artifacts. Figure 12 shows the measured and predicted MSE line ratios in function of electron density. Although the minimum electron density that was obtained, is not low enough to do an accurate check on the electron density scaling, the agreement with the modelled line ratios that were obtained with Marchuk et al.'s CR model [4] is very good and the deviation with the statistical line ratios is clear.

The use of the ratio between the observed σ and π radiance to obtain information on the direction of the Lorenz field, and hence on the magnetic pitch angle, has rarely been successful. This is mainly due to the non-statistical features in the MSE spectrum. The classical polarization based MSE diagnostic [43] is much less sensitive to this effect, except when σ and π lines overlap in the sampled wavelength region. In this case a change in electron density could change the amount of σ and π light which is sampled. In Fig.13 the modelled total σ and π-emissivity is plotted in function of electron density for a beam energy of 55keV/amu. The difference with the statistically expected ratio can be as high as 20% for standard tokamak conditions. In order to compare with the experimentally observed ratio, the disturbing effect of the geometry and the polarization sensitivity of the first mirror was obtained using the ratio between the σ 1- and π3-lines. These originate from the same upper level and hence $\Phi_{\sigma 1}/\Phi_{\pi 3}$ is independent of the population structure. However, because the Stark splitting is usually not large enough, it is in practical situations difficult to obtain this ratio with the accuracy that is needed for direct use as a constraint on the magnetic field reconstruction. The measurements compare well to the model, but the use of $\Phi_{\sigma 1}$ and $\Phi_{\pi 3}$ induces considerable statistical noise.

In Fig. 14, the expected measurement $\Phi_{\sigma 1}/\Phi_{\pi 3}$ is plotted in function of the angle between a line of sight and the Lorentz field taking into account the effects of the n = 3 non-statistical population and a first mirror with an s-reflectivity which is 15% larger than the p-reflectivity. This value was obtained from the $\Phi_{\sigma 1}/\Phi_{\pi 3}$ ratio and the known beam and l.o.s. geometry during a beam into gas shot for which the magnetic field is purely toroidal. One can see that the main effect that causes a deviation between the simple geometrical prediction ($\Phi_\sigma / \Phi_\pi = (1 + \cos^2\theta) / \sin^2\theta$) and the measurements is the non-statistical character of the n = 3 population. The measured points agree very well to the modelled curves, however for the equatorial viewing geometry used here, this method cannot be used to obtain useful information about θ (and hence the magnetic pitch angle), because a large change in θ is needed to cause a measurable change in Φ_σ / Φ_π.

CONCLUSIONS

In this paper we have analysed the consistency of several collisional-radiative models [1, 2, 3] that have been developed to calculate the neutral beam stopping and population of excited states in hydrogen plasmas. The results of the calculations are compared with experimental data from JET. Revisiting the proton impact ionization of excited states and identification of a mistake in the ADAS rescaling of the charge exchange cross sections allowed us to achieve consistency between all models. The corrected data will be in a next ADAS release. The calculated relative n = 3 to n = 4 population agrees within 10% to the measured ratio from JET using the H_α to H_β beam emission intensities. Good agreement is found as well on the power fractions measured with BES and on the JET Neutral Beam Test Bed, if a correction to the analysis in [40, 41] is taken into account. The power fractions measured with neutral beam in gas emission show a sligthly larger deviation. The radial profiles and time traces of the measured and modelled NB density agree well but the overall intensity of the measured beam density is ≈30% lower. The reason for this is uncertain, but could also be due to a combination of calibration, characterization of the beam and alignment between

line of sight and neutral beam rather than due to the atomic data itself. Many of these issues are currently the main motivation to use beam emission. The Stark line intensities within the MSE multiplet are in good agreement with a sublevel resolved model [4]. The measured σ/π intensity is disturbed by the polarization characteristics of the tokamak side optics and the $n = 3$ sub population structure, the latter effect is consistent with the CR modelling.

The overall agreement found on JET between the modelled and expected beam emission intensities gives confidence in the proposed scheme combining charge exchange and beam emission that will be used to measure the helium ash on ITER. The agreement between the modelled and measured MSE spectra gives confidence in the Stark resolved CR modelling and hence such a model could be used to correct the measured σ/π-ratio when used to constrain magnetic field reconstructions.

ACKNOWLEDGEMENT

This work was supported by EURATOM and carried out within the framework of the European Fusion Development Agreement. The views and opinions expressed herein do not necessarily reflect those of the European Commission.

REFERENCES

[1]. H. Anderson, M. Fig von Hellermann, R. Hoekstra, L.D. Horton, A.C. Howman, R.W.Fit. Konig, R. Martin, R.E. Olson, and H.P. Summers. Plasma Physics and Controlled Fusion, **42**:781{806, 2000.

[2]. I.H. Hutchinson. Plasma Physics and Controlled Fusion, **44**(1):71{82, 2002.

[3]. O. Marchuk, Fig. Bertschinger, W. Biel, E. Delabie, M. Fig. von Hellermann, R. Jaspers, and D. Reiter. Review of Scientific Instruments, **79**(10):10F532, 2008.

[4]. O. Marchuk, Yu Ralchenko, R.K. Janev, W. Biel, E. Delabie, and A.M. Urnov. Journal of Physics B-Atomic Mololecular and Optical Physics, **43**(1):011002, 2010.

[5]. R.K. Janev, C.D. Boley, and D.E. Post. Nuclear Fusion, **29**:2125{2140, 1989.

[6]. S. Suzuki, Fit. Shirai, M. Nemoto, K. Tobita, H. Kubo, Fit. Sugie, A. Sakasai, and Y. Kusama. Plasma Physics and Controlled Fusion, **40**(12):2097{2111, 1998.

[7]. R.P. Seraydarian, K.H. Burrell, and R.J. Groebner. Review of Scientific Instruments, **59**(8):1530{1532, 1988.

[8]. A. Boileau, M. Von Hellermann, L.D. Horton, J. Spence, and H.P. Summers., Plasma Physics and Controlled Fusionn, **31**(5):779{804, 1989.

[9]. W. Mandl, R.C. Wolf, M.Fig von Hellermann, and H.P .Summers. Plasma Physics and Controlled Fusion, **35**:1373{1394, 1993.

[10]. M.Fig. von Hellermann, R.J.E. Jaspers, H.P. Summers, and K-D Zastrow. Advanced diagnostics for magnetic and inertial fusion. edited by P Stott et al., Kluwer Academic, N.Y., 125-128, 2001.

[11]. M.De Bock, K. Jakubowska, M.Fig. von Hellermann, R.J.E. Jaspers, A.J.H. Donne, and L. Shmaenok. Review of Scientific Instruments, **75**:4155{4157, 2004.

[12]. R. J. E. Jaspers, M. Fig. von Hellermann, E. Delabie, W. Biel, O. Marchuk, and L. Yao. Review of Scientific Instruments, **79**(10):10F526, 2008.

[13]. W.L. Rowan, M.B. Sampsell, and R.S. Granetz. Review of Scientific Instruments, **75**:3487{3489, 2004.
[14]. H Euringer and Ph Verplancke. Review of Scientific Instruments, **65**:2996{2999, 1994.
[15]. C. Giroud, A.Fig. Meigs, C.R. Negus, K.D. Zastrow, T.M. Biewer, Fit.W. Versloot, and JET-EFDA Contributors. Review of Scientific Instruments, **79**(10):10F525, 2008.
[16]. K. Jakubowska, M.De Bock, R Jaspers, M.Fig. Von Hellermann, and L Shmaenok. Review of Scientific Instruments, **75**(10):3475{3477, 2004.
[17]. N.A. Pablant, K.H. Burrell, R.J. Groebner, D.H. Kaplan, and C.Fit. Holcomb. Review of Scientific Instruments, **79**(10):10F517, 2008.
[18]. R.C. Wolf, L-G Eriksson, M.Fig. Von Hellermann, R. Konig, W. Mandl, and F. Porcelli. Nuclear Fusion, **33**(12):1835, 1993.
[19]. E.L. Foley, F.M. Levinton, H.Y. Yuh, and L.E. Zakharov. Review of Scientific Instruments, **79**(10), 2008.
[20]. C.D. Boley, R.K. Janev, and D.E. Post. Physics Review Letters, **52**(7):534{537, 1984.
[21]. R.K. Janev and J. Smith. Atomic Plasma Materials Int. Data Fusion, 1993.
[22]. P.D. Fainstein, V.H. Ponce, and R.D. Rivarola., Journal of Physics B-Atomic Mololecular and Optical Physics, **23**(9):1481{1489, 1990.
[23]. A. Igarashi and Fit. Shirai. Physical Review A, **50**(6, Part A):4945{4950, 1994.
[24]. M. McCartney and D.S.F Crothers. Zeitschrift fur Physik D-Atoms Molecules and Clusters, **35**(1):1{2, 1995.
[25]. Fig.H. Olivera, R.D. Rivarola, and P.D. Fainstein. Physical Review A, **51**(1):847{849, 1995.
[26]. ALADDIN database maintained by the IAEA. http://www-amdis.iaea.org/aladdin.
[27]. M. O'Mullane. http://www.adas.ac.uk/notes/adas c09-01.pdf.
[28]. H.P. Summers. The ADAS User Manual, version 2.6, http://adas.phys.strath.ac.uk. 2004.
[29]. E.Y. Sidky and C.D. Lin. Physical Review A, **65**(1):012711, 2001.
[30]. A. Kolakowska, M.S. Pindzola, and D. R. Schultz. Physical Review A, **59**(5):3588{3591, 1999.
[31]. Nobuyuki Toshima. Physical Review A, **59**(3):1981{1987, 1999.
[32]. Thomas Fig. Winter. Physical Review A, **80**(3):032701, 2009.
[33]. M.B. Shah and H.B Gilbody. Journal of Physics B-Atomic Mololecular and Optical Physics, **14**(14):2361{2377, 1981.
[34]. M.B. Shah, D.S. Elliott, and H.B. Gilbody. Journal of Physics B-Atomic Mololecular and Optical Physics, **20**(11):2481{2485, 1987.
[35]. M.F. Gu, C.Fit. Holcomb, R.J. Jayakuma, and S.L. Allen. Journal of Physics B-Atomic Mololecular and Optical Physics, **41**(9):095701, 2008.
[36]. B.H. Bransden and McDowell M.R.C. Charge Exchange and the Theory of Ion-Atom Collisions. Clarendon Press, Oxford, 1992.
[37]. Yu Ralchenko and Y Maron. Journal of Quantitative Spectroscopy Radiative Transfer, **71**(2-6):609{621, 2001.
[38]. C.R. Negus, C. Giroud, A.Fig. Meigs, K.D. Zastrow, D.L. Hillis, and JET-EFDA Contributors. Review of Scientific Instruments, **77**(10):10F102, 2006.

[39]. D. Ciric, J.J. Milnes, and E. Surrey. Misalignment on multi-aperture particle beam properties. 19th IEEE/NPSS Symposium on Fusion Engineering, 2002.

[40]. R.S. Hemsworth. JET-DN-C(85)**8**, 1985.

[41]. R. Uhlemann, R.S. Hemsworth, Fig. Wang, and H. Euringer. Review of Scientific Instruments, **64**:974{982, 1993.

[42]. I.D. Williams, J. Geddes, and H.B. Gilbody. Journal of Physics B-Atomic Mololecular and Optical Physics, **15**:1377{1389, 1982.

[43]. F.M. Levinton, R.J. Fonck, Fig.M. Gammel, R. Kaita, H.W. KugelL, ET Powell, and DW Roberts. Physics Review Letters, **63**(19):2060{2063, 1989.

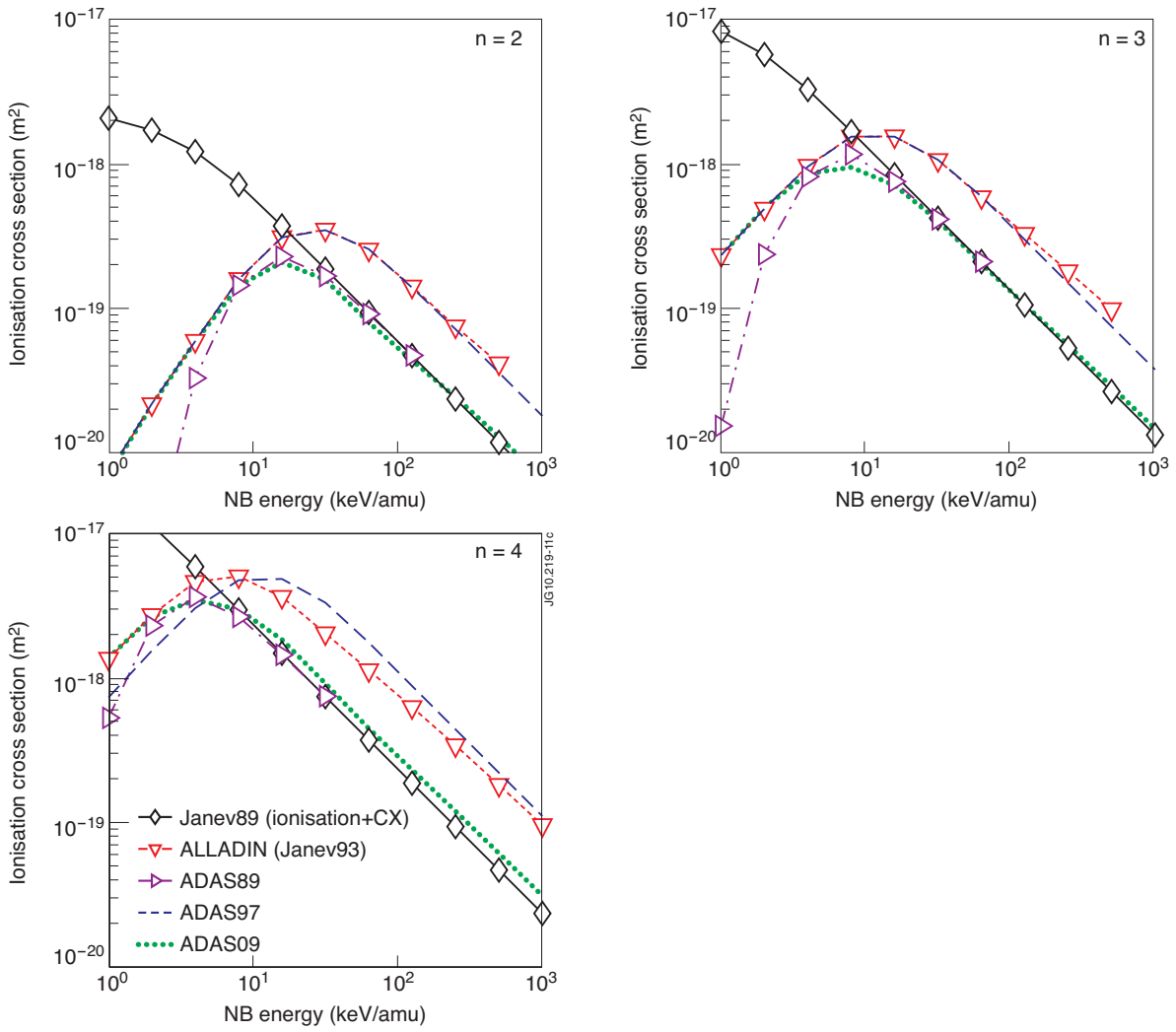

Figure 1: Proton impact ionization of excited states of the hydrogen atom. Recommended data sets (Janev89 [5] and Janev93 (as in the ALLADIN database) [21, 26]) and data used in the ADAS beam emission models are shown.

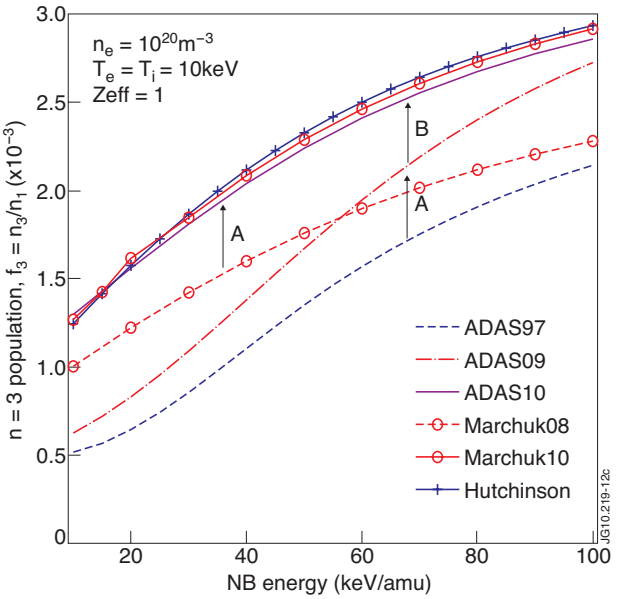

*Figure 2: n = 3 population in the beam with regard to the ground state according to dierent CR models. ADAS: ADAS excited beam population [1, 28]; Marchuk: n = 3 population from Marchuk et al.[3]; Hutchinson: excited population digitised from Fig.3 in Hutchinson [2]. **A** denotes the change due to the correction of H(n>1) ionization, **B** marks the change due to a correction of H(n>1) charge exchange in ADAS.*

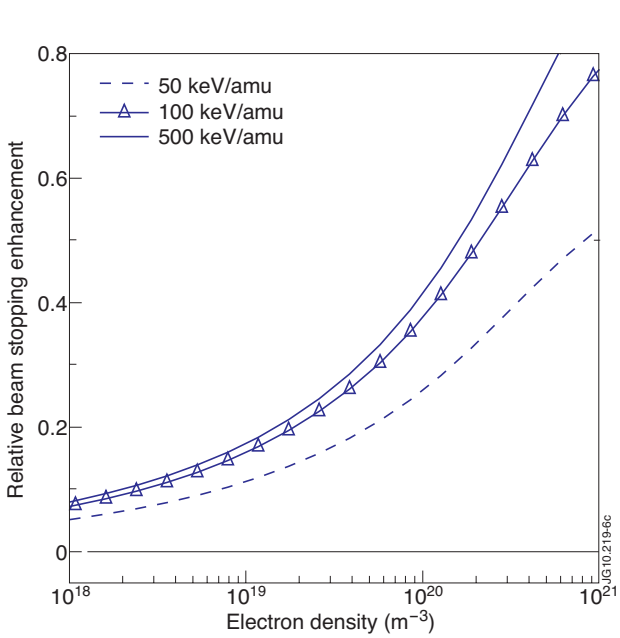

(a) Relative increase of the beam stopping cross section due to stepwise ionization trough excited states in function of electron density, using the CR model of Marchuk et al. [3]. ($T_e = T_i = 5keV$, $Z_{eff} = 1$)

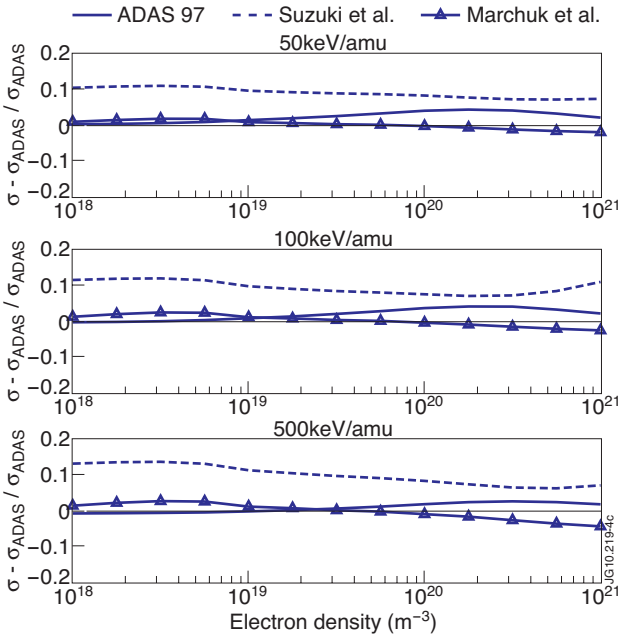

(b) Comparison of NB stopping cross sections from several CR models for the NB. The difference due to the correction of the excited state ionization and charge exchange is also shown. ($T_e = T_i = 5keV$, $Z_{eff} = 1$)

Figure 3: The role of excited states in NB stopping and consistency of beam stopping cross sections from several models.

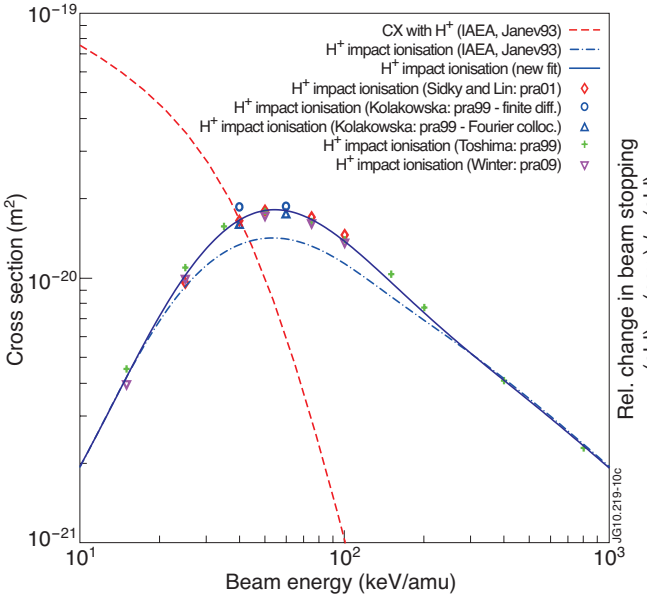

(a) Recommended data for ionization and charge exchange compared with data from recent theoretical publications [29, 30, 31, 32].

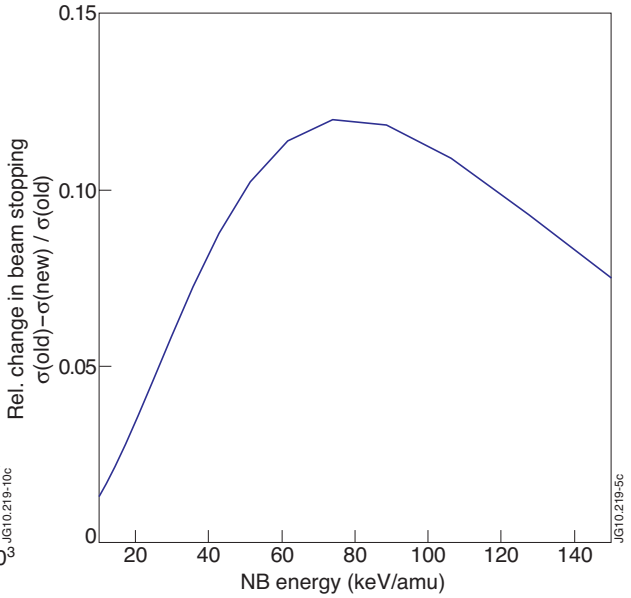

(b) Impact of the change in ion impact ionization on the NB stopping cross section. ($T_e = T_i = 5keV$, $Z_{eff} = 1$)

Figure 4: Recent theoretical results on the cross sections for H^+ impact ionization and charge exchange of H(1s), and the impact on the effective beam stopping cross sections.

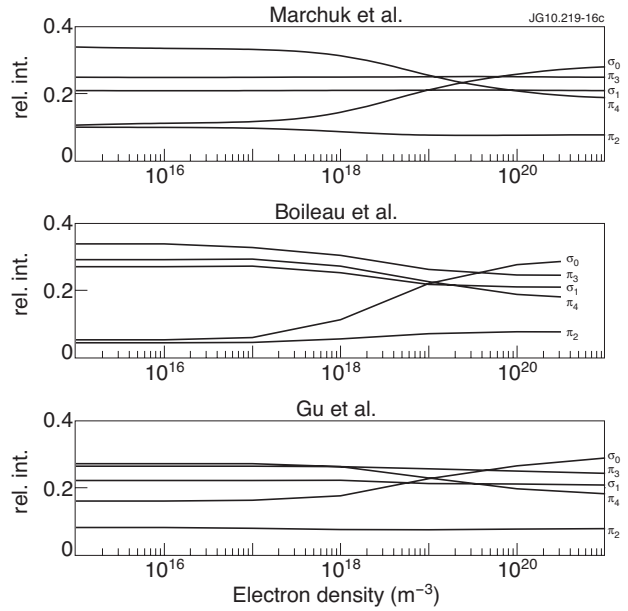

(a) Line ratios within the MSE mulitplet from several Stark resolved CR models [4, 8, 35].

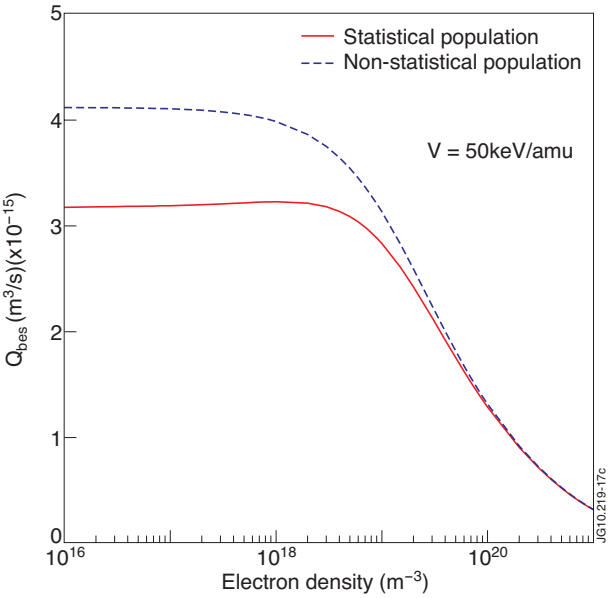

(b) Comparison of the H beam emission rate for the (nkm)- and n-resolved CR model of Marchuk et al. [4] (restricted to n = 5, V = 55keV/amu,$T_e = T_i = 5keV$)

Figure 5: Effect of Stark level resolved modelling on the MSE line ratios and on the total H_α beam emission rate.

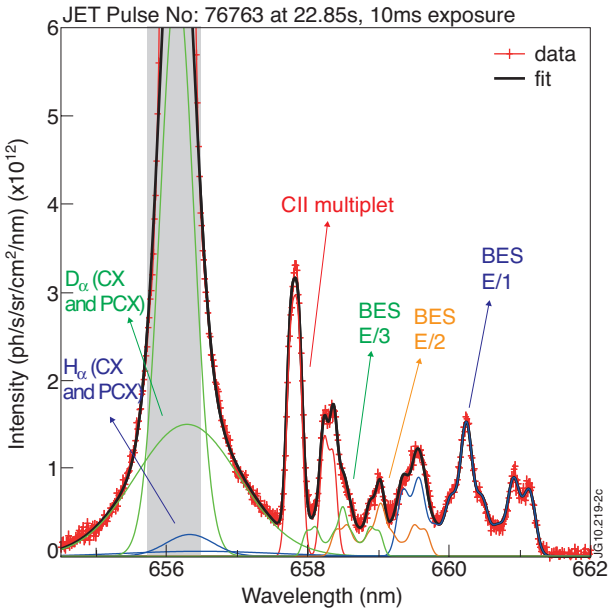

Figure 6: D_α spectrum from JET, the experimental data is in red, other lines are fitted features. The three energy components of the BES spectrum are indicated. The active and passive D/H CX contributions are approximated as gaussian lines. The coldest part of the D/H spectrum (the grey area) is usually overexposed and is neglected in the fit.

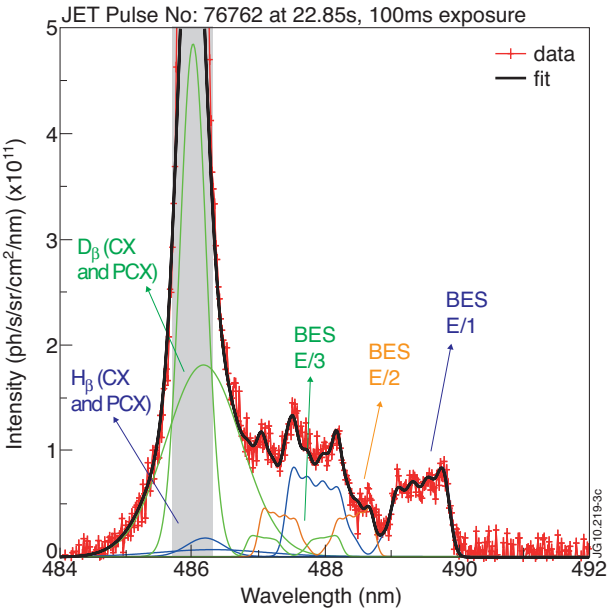

Figure 7: Example D_β spectrum from JET. The coldest part of the D/H spectrum (the grey area) is neglected in the fit.

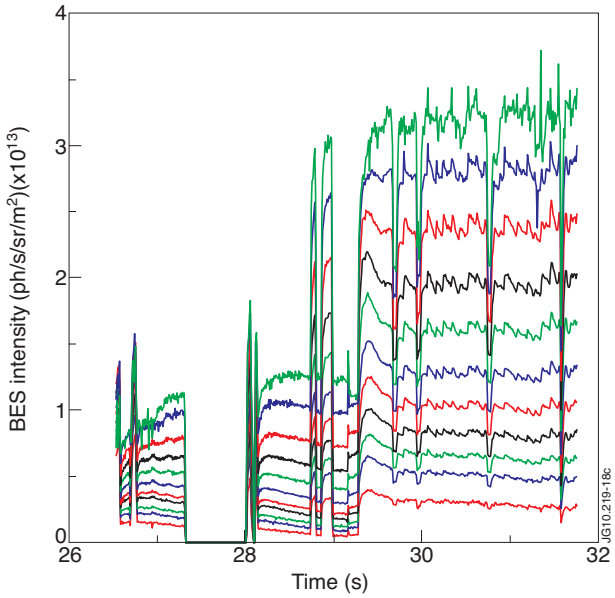

a) Beam emission intensity of the full energy component for Pulse No: 72324 along several lines of sight of the JET core CXRS diagnostic. Two beams contribute to the beam emission spectrum.

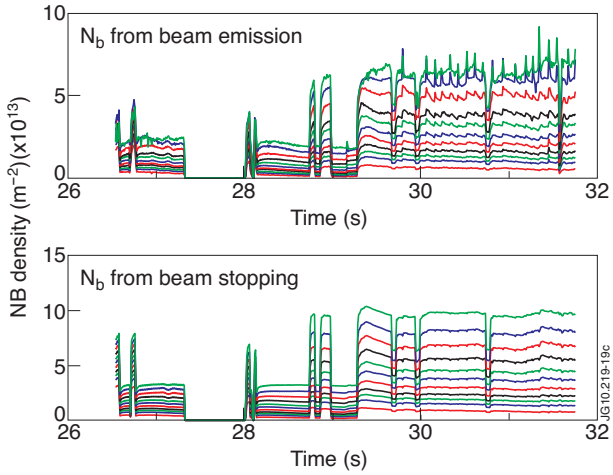

(b) Time traces of the line integrated NB density (E/1 component) derived from beam emission (top) and from a NB attenuation code (bottom) for Pulse No: 72324. Two beams contribute to the line integrated beam density.

Figure 8: Time traces of the beam emission intensity and the beam density along a line of sight (E/1 component beam 8.7 + 8.8).

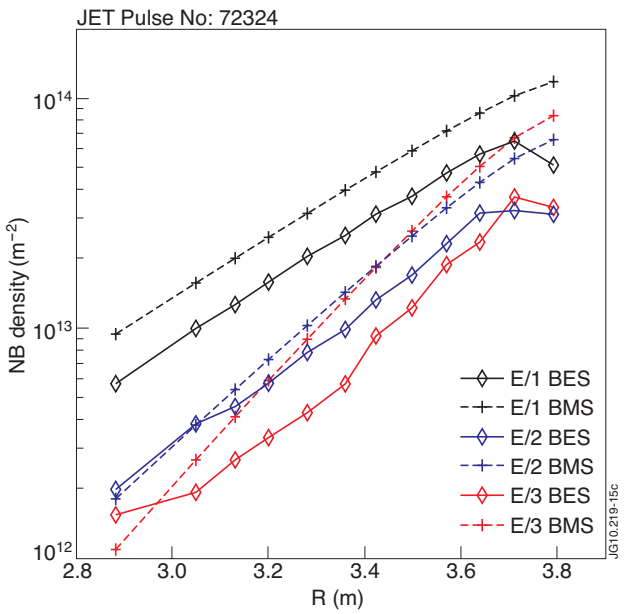

(a) Profile of the NB density integrated along a L.O.S for the three energy fractions in the beam for Pulse No: 72324 at 30.3s. 'BES' refers to measured data using beam emission, 'BMS' is the expectation from a beam stopping code.

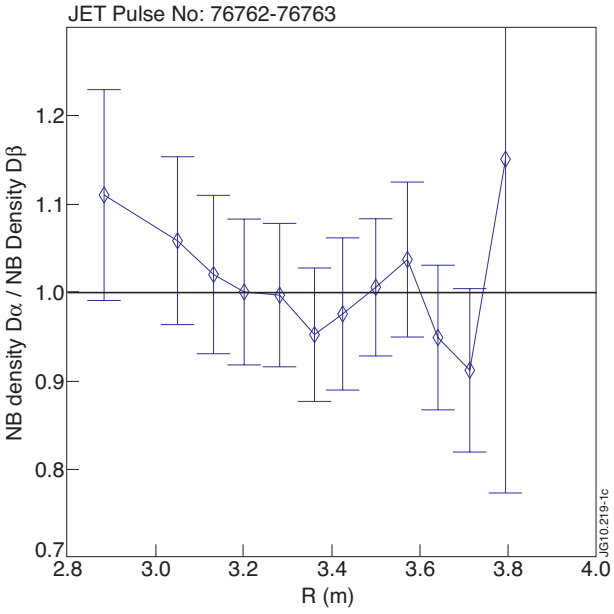

(b) Ratio of NB densities measured on D_α and D_β beam emission from two similar discharges. The NB attenuation code predicts a maximum dierence between the shots of approximately 5% at this time frame. The beam density measured on D_α is consistent with the beam density measured on D_β.

Figure 9: Consistency between beam densities from beam emission and the expected NB density from a beam attenuation code (Pulse No: 72324) and consistency between D_α and D_β.

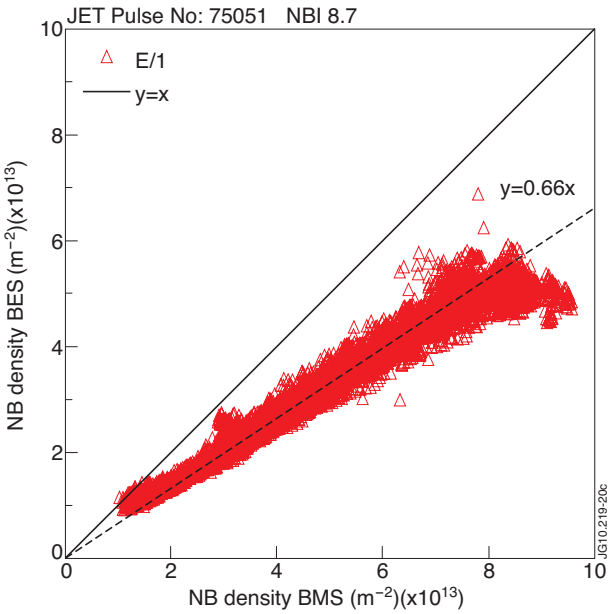

Figure 10: NB density from BES against the beam stopping (BMS) prediction for beam 8.7 (Pulse No: 75051). The odd edge channel is neglected.

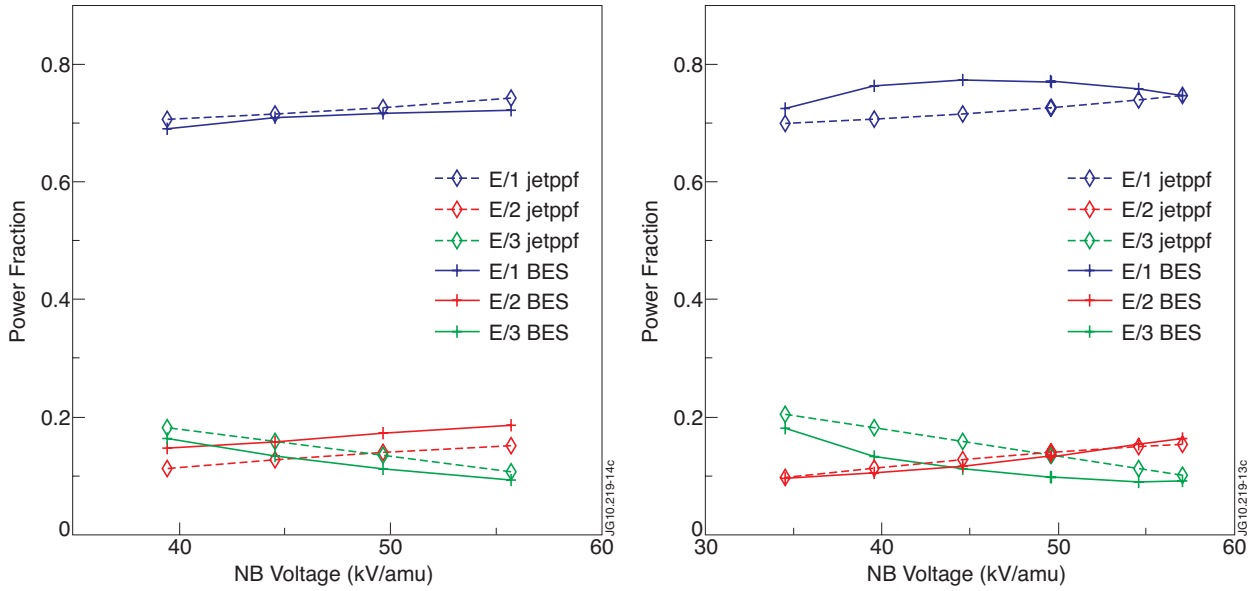

(a) The data labelled 'BES' is from beam emission in plasma (Pulse No's: 75046-75050), the data labelled 'jetppf' shows the expected power fractions.

(b) The data labelled 'BES' is from beam in gas emission (Pulse No's:77528-77534), the data labelled 'jetppf' shows the expected power fractions.

Figure 11: Distribution of the power among the fractional energy components in the NB, in function of beam voltage. The power fractions measured with beam emission are compared with the expected fractions from a model based on test bed measurements.

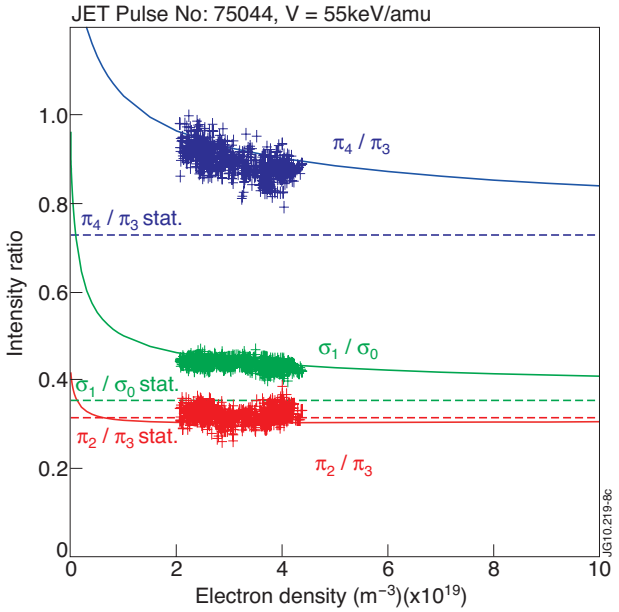

Figure 12: Stark line ratios within the MSE multiplet in function of electron density. Data from a central track of the JET core CXRS diagnostic (MSE multiplet best resolved) is compared with the model from Marchuk et al. [4]. The dashed lines show the expected line ratios when the n = 3 level would have a statistical subpopulation.

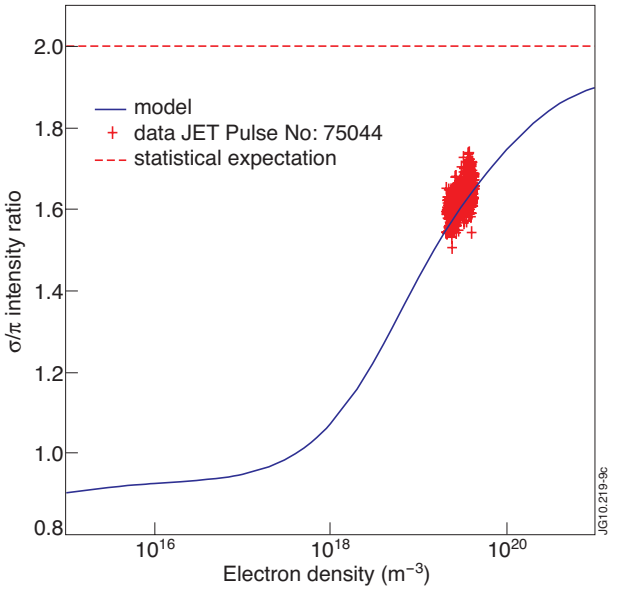

Figure 13: Ratio between the total σ- and π-emissivity (integrated over all solid angles). The experimental data points have been obtained from the measured σ- and π-radiances through $\frac{I_\sigma}{I_\pi} = \frac{\Phi_\pi}{\Phi_\pi} \Big/ \frac{\Phi_{\sigma 1} A_{\pi 3}}{\Phi_{\pi 3} A_{\sigma 3}}$ *The label 'model' refers to the model of Marchuk et al. [4]. The dashed line shows the statistical prediction* $I_\sigma = 2I_\pi$.

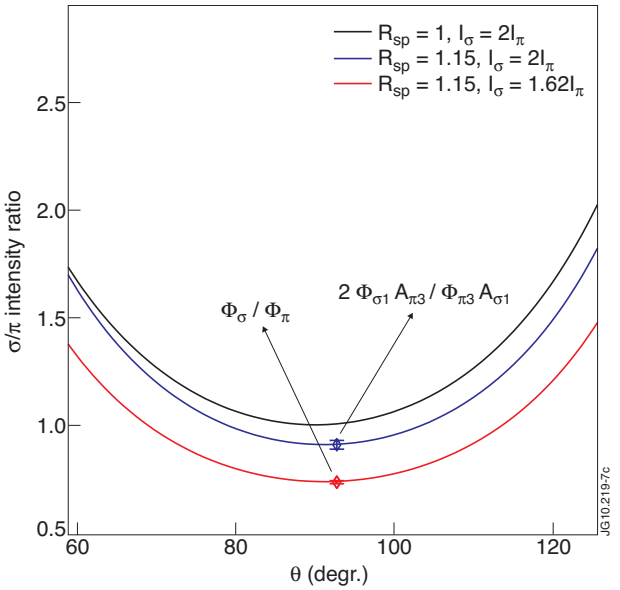

Figure 14: Ratio of the expected σ- over π-radiance in function of angle θ between a core line of sight and the Lorentz field. R_{sp} is the ratio between the s-and p- reflecivity of the first mirror. The case $R_{sp} = 1$, $I_\sigma = 2I_\pi$ corresponds to the standard prediction $\Phi_\sigma / \Phi_\pi = (1 + \cos^2 \theta) / \sin^2 \theta$. The blue and red curve correspond to the situation with a polarization sensitive first mirror and with a n = 3 population that has not reached a statistical distribution. The points indicate measurements from JET Pulse No: 75044. For this viewing geometry a large change in is needed to cause an appreciable change in the measured Φ_σ / Φ_π intensity ratio.